

**Elastic, Viscoelastic and Fibril-reinforced Poroelastic Material
Properties of Human Tibial Cartilage**

Mohammadhossein Ebrahimi
Master's Thesis
Master's degree in medical physics programme
University of Eastern Finland
Department of Applied Physics
13.04.2018

University of Eastern Finland, Faculty of Science and Forestry

Master's degree in medical physics programme

Mohammadhossein Ebrahimi, B.Sc.: Elastic, Viscoelastic and Fibril-reinforced Poroelastic Material Properties of Human Tibial Cartilage

Master's thesis, 64 pages

Supervisors: Petri Tanska, Ph.D.

Simo Ojanen, M.Sc.

Professor Rami Korhonen, Ph.D.

April 2018

Keywords: Articular cartilage, Osteoarthritis, Mechanical testing, Fibril-reinforced poroelastic material, Finite element analysis

Abstract:

Articular cartilage, covering the endplates of the bones, provides smooth movements in the human joints. The main cartilage tissue constituents contributing in mechanical function of tissue are proteoglycans, collagen fibers network and interstitial fluid. Osteoarthritis (OA), which is prevalent joint disorder, affects the composition and structure of cartilage and consequently these changes triggers reduction of loading capacity of cartilage.

In this study, human tibial cartilage samples were harvested from cadaver knee joints. The International Cartilage Repair Society (ICRS) scores, indicating the degeneration level of cartilage in the knee joint, were associated to each cartilage sample. Biomechanical properties of the samples were measured using indentation device through stress-relaxation and cyclic loading-unloading protocols. The equilibrium and dynamic moduli were calculated accordingly. Following that, the Finite Element (FE) models of samples were constructed. Cartilage was modeled as a fibril-reinforced poroelastic (FRPE) material, which is capable to distinguish the main constituents of cartilage tissue. The material parameters were optimized so that the experimental measurement had the best match with FE-obtained data. The samples were classified into two different groups (presumably healthy or OA), using the ICRS score or equilibrium modulus.

The dynamic modulus showed the lowest value of 0.97 ± 0.80 MPa at 0.005 Hz, followed by a rapid increase and finally reaching a plateau (1.3 ± 0.05 MPa) at the frequencies corresponding routine daily activities. Similarly, the phase difference was highest at 0.005 Hz ($19.3 \pm 4.9^\circ$), followed by a phase difference plateau ($7 \pm 0.48^\circ$) at the frequencies corresponding routine daily activities. These indicate that the dynamic properties of cartilage are constant at the frequency range of routine daily activities. In the ICRS-based grouping, none of the investigated parameters were significantly different between the presumably healthy and OA groups. Whereas, in the equilibrium modulus-based grouping, the presumably OA group had lower dynamic modulus and higher phase difference compared to the presumably healthy group, indicating degeneration in the collagen network and/or changes in the fluid pressurization capability of cartilage. Furthermore, the presumably healthy group had higher strain-dependent fibril network and non-fibrillar matrix moduli, suggesting that the proteoglycan matrix and collagen network were in better condition. In addition, permeability in the presumably OA group was significantly higher compared to the presumably healthy group, showing the stage of higher cartilage degeneration in the OA group

In conclusion, the findings of the current study confirm that the ICRS-based grouping of the samples is not able to reveal biomechanical changes during OA development, most likely because the ICRS scoring concerns visible cracks and fibrillation, which do not necessarily reflect OA changes that potentially occur in deeper cartilage. Whilst, the FRPE and dynamic material properties of cartilage were shown to reflect the OA development when the samples were grouped based on their bulk equilibrium modulus.

Abbreviations:

ECM	Extracellular matrix
FRPE	Fibril-reinforced poroelastic
GAG	Glycosaminoglycan
ICRS	International Cartilage Repair Society
OA	Osteoarthritis
PG	Proteoglycan

Symbols:

E_{eq}	Equilibrium modulus
H_A	Aggregate modulus
k_H	Hydraulic permeability
ν	Poisson's ratio
$E_{storage}$	Storage modulus
E_{loss}	Loss modulus
σ_0	Peak-to-peak value of the stress in dynamic test
ε_0	Peak-to-peak value of the strain in dynamic test
δ	The phase difference between the sinusoidal stress and strain curves in dynamic test
E_{dyn}	Dynamic modulus
C^E	Stiffness matrix
σ_{ii}	Stress in the direction ij
ε_{ii}	Strains in the direction ij
E	Young's modulus
G_{ij}	The shear modulus in the direction ij
ν_{ij}	Poisson's ratio in the direction ij
n_s	Relative solid volume fractions
n_{fl}	Relative fluid volume fractions
p	Fluid pressure

σ_{eff}	The effective solid matrix stress
σ_{tot}	Total stress tensor
q	The rate of the fluid flow
∇p	The fluid pressure gradient
k	Permeability
k_0	Initial permeability
e	Void ratio
e_0	Initial void ratio
M	Permeability strain-dependency coefficient (dependent on void ratio)
σ_{nf}	Stress in the non-fibrillar matrix
σ_f	Stress in the fibrillar matrix
K	Bulk modulus
F	Deformation gradient tensor
J	Determinant of the deformation tensor
E_{nf}	Non-fibrillar matrix Young's modulus
ν_{nf}	Non-fibrillar matrix Poisson's ratio
$\sigma_{f,p}$	Primary fibrils stress
$\sigma_{f,s}$	Secondary fibrils stress
C	Fraction of primary fibrils to the secondary fibrils
ρ_z	Depth-dependent collagen fraction per the solid volume
f_{tot}	The total number of individual fibers
σ_f^i	The stress in the individual fiber
σ_f	Total fibrillar stress
ϵ_f	The fibril strain
E_f	Young's modulus of the fibrillar network
E_f^0	The initial fibril network modulus
E_f^ϵ	Strain-dependent fibril network modulus

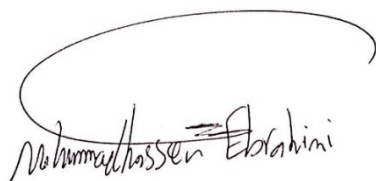
$\delta\bar{F}$	Objective function
F_i^{sim}	Simulated values in optimization function
F_i^{exp}	Experimental values in optimization function
$F_{i,p}^{\text{sim}}$	Peak force values obtained from simulation
$F_{i,p}^{\text{exp}}$	Peak force values obtained from experiment

Preface:

This master's thesis was conducted at University of Eastern Finland, Department of Applied Physics, Biophysics of Bone and Cartilage (BBC) research group. This thesis aimed to characterize human tibial cartilage in order to increase our knowledge from tissue mechanical properties and functional alteration of tissue as it develops osteoarthritis.

I would like to thank everyone who participated in this study. I want to thank my supervisor professor Rami Korhonen who has given me the chance to work with him. I am grateful to my supervisor, post-doctoral researcher Petri Tanska who has provided me with new ideas and perspectives, taught me patiently and shared with me his invaluable expertise needed for this work. I would like to thank my other supervisor, Simo Ojanen who helped me with my experiments. I am thankful to Professor Petro Julkunen for reviewing my thesis. I would deeply appreciate my best friend, Ali Mohammadi for all his help during my master's degree.

I would express my deepest gratitude towards my wonderful parents and brother for providing me with the possibility to travel thousands of kilometers away from home to study, develop my skills and gain knowledge. I am forever grateful for the security and help they have provided throughout my life.

A handwritten signature in black ink, reading "Mohammadhossein Ebrahimi". The signature is written in a cursive style and is enclosed within a large, thin, hand-drawn oval shape.

Mohammadhossein Ebrahimi

April 13, 2018. Kuopio, Finland

Contents

1.	Introduction.....	10
2.	Background.....	12
2.1	The knee joint	12
2.2	The structure and composition of articular cartilage.....	13
2.2.1	Collagen network	14
2.2.2	Proteoglycans	15
2.2.3	Interstitial fluid.....	15
2.3	Mechanical function and properties of cartilage	16
2.4	Osteoarthritis and its effects on tissue structure.....	17
2.5	Biomechanical characterization of articular cartilage.....	18
2.5.1	Mechanical testing configurations	19
2.5.2	Loading protocols	20
2.5.2.1	Creep	20
2.5.2.2	Stress-relaxation.....	20
2.5.2.3	Dynamic.....	22
2.6	Computational modeling of articular cartilage	23
2.6.1	Isotropic and transversely isotropic linear elastic materials.....	23
2.6.2	Biphasic materials	24
2.6.3	Fibril-reinforced biphasic and poroelastic materials.....	25
2.6.3.1	Non-fibrillar matrix.....	26
2.6.3.2	Fibrillar matrix	27
2.7	Optimization of the material parameters.....	29
3.	Materials and methods	31
3.1	Sample preparation	31
3.2	Biomechanical indentation test	32
3.2.1	Stress relaxation data preprocessing	33
3.2.2	Equilibrium modulus acquisition	34
3.3	Dynamic tests data analysis	35
3.4	Finite element analysis.....	36
3.5	Material parameter optimization.....	37
3.6	Data analysis	38
3.6.1	ICRS (visual inspection-based) grouping	38
3.6.2	Equilibrium modulus based grouping	39
3.6.3	Statistical Analysis.....	40
4.	Results.....	41

4.1	Elastic behavior of human tibial cartilage.....	41
4.2	Viscoelastic behavior of human tibial cartilage.....	41
4.2.1	ICRS-based grouping.....	43
4.2.2	Equilibrium modulus based grouping.....	44
4.3	FRPE material properties.....	45
4.3.1	ICRS-based grouping.....	45
4.3.2	Equilibrium modulus based grouping.....	45
5.	Discussion.....	47
	Appendix A.....	51
	Appendix B.....	53
	Bibliography.....	55

Chapter 1

Introduction

Articular cartilage is a connective tissue and it provides lubricated surface and low friction movement for articular joint. Articular cartilage has no nerves, lacks enough vascularization and thus possesses a low regeneration and healing capacity. The only cell type within the tissue is chondrocyte, which is almost immobile cell due to being trapped in the extracellular matrix (ECM) [1].

There are some studies evaluating articular cartilage through various methods such as spectroscopical [2], histological [3] or biomechanical [3,4] characterization methods in different scales including macro-level [4], micro-level [5] and most recently nano-level [6]. There are several measurement methods for quantifying mechanical properties of cartilage tissue such as confined, unconfined or indentation test, aiming to quantify the bulk mechanical properties of cartilage via stress-relaxation [7], creep [8] or dynamic measurement protocols [9]. The macro-level tissue material properties, including aggregate modulus, dynamic modulus and Poisson's ratio, have been extensively studied [3,4].

The constituents of articular cartilage control its mechanical function. The main constituents are collagen network (50-80% of dry weight), proteoglycans (PGs, 30% of dry weight) and highly viscous interstitial fluid (60-85% of total tissue wet-weight) [10,11]. During the instantaneous loads or cyclic loading of cartilage, the interstitial fluid pressurization and collagen fibers contribute most to the mechanical response of cartilage [12]. However, if the cartilage is under static loading, the interstitial fluid flows out of the tissue and the negatively charged proteoglycan matrix mainly controls the mechanical response of cartilage. Cartilage porosity and interstitial fluid flow mainly determine its time-dependent properties. However, collagen fibers viscosity contributes in time-dependent properties as well. The PGs and collagen fibers restrict the fluid flow directionally [4].

Osteoarthritis (OA) is a degenerative joint disease. Progression of OA can be caused due to either non-identifiable causes (idiopathic) or trauma (post-traumatic OA). There are some well-identified risk factors associated with OA, including obesity, lack of mobility and unhealthy lifestyle. According to the literature, regular moderate exercises can be useful for prevention of OA development [13]. Currently, there are no pharmaceutical treatments for severe cartilage degeneration at the latest stages of OA. Regarding the OA diagnosis, arthroscopy is capable of determining osteoarthritic cartilage tissue. International Cartilage Repair Society (ICRS) has defined a grading system for OA characterization, in which arthroscopy is used to visually score the cartilage health status [3].

Cartilage constituents undergo substantial changes during the onset and progression of OA. Fibrillation of the collagen network and PG loss are frequently reported to occur during early stages of OA [5]. As OA progresses, collagen and PG content are further reduced, leading to increased fluid content and tissue swelling. These changes also increase permeability of the tissue and together they result in decreased equilibrium and dynamic moduli of the articular cartilage [4,14]. At the latest stages of OA, when the capacity of articular cartilage to bear cyclic and prolonged loads has significantly decreased, the articulating surfaces of a joint start to wear out, causing a painful bone-on-bone contact.

There are several computational material models for simulation of the mechanical function of soft tissues. Among those, fibril-reinforced poroelastic (FRPE) material model is able to mimic the experimental measurements accurately [15]. This material model has been applied extensively to characterize various animal cartilage samples, but has not been used widely for human [15–17]. The realistic human cartilage material properties, applied to computational models (e.g. knee), are more representative of the function of human tissues.

The alterations of the tissue properties at different stages of OA have received a great research focus. However, most of the studies have focused on animal cartilage and have not used state-of-the-art computational methods for investigating the roles of material constituents on the mechanical behavior of cartilage at different stages of OA. Therefore, the aim of this Master's thesis is **I**) to characterize the mechanical properties of human tibial cartilage by investigating the mechanical behavior via dynamic and stress-relaxation measurements in indentation and **II**) to characterize FRPE material properties with finite-element modeling utilizing aforementioned experimental indentation measurements. We hypothesize that the alterations of tissue material properties can interpret the progression of OA as characterized by the visual OA grading and biomechanical-based grouping. The study provides novel information of mechanical properties of human tibial cartilage and their alterations during the progression of OA

Chapter 2

Background

2.1 The knee joint

The synovial joints in the human body are the most mobile joints facilitating the human motion. There are different types of synovial joints in the human body including gliding joint, pivot joints, saddle joints, ball and socket joints and hinge joints [18]. The knee joint, which is a hinge joint, is the largest hinge joint and one of the most complex joint functionally.

The knee joint connects three bones, that are tibia, femur and patella, through two different mechanisms called as tibiofemoral and patellofemoral joints [19]. The main function of the knee joint is to provide smooth rotations and translations between tibia and femur [20]. The bones are connected together with the connective soft tissues including muscles, ligaments and tendons. The main roles of the ligaments are to provide joint stability and to absorb the shock loadings. The function of tendons is to transmit forces from muscles to bones [21]. Figure 2.1 depicts the anatomy of the human knee joint.

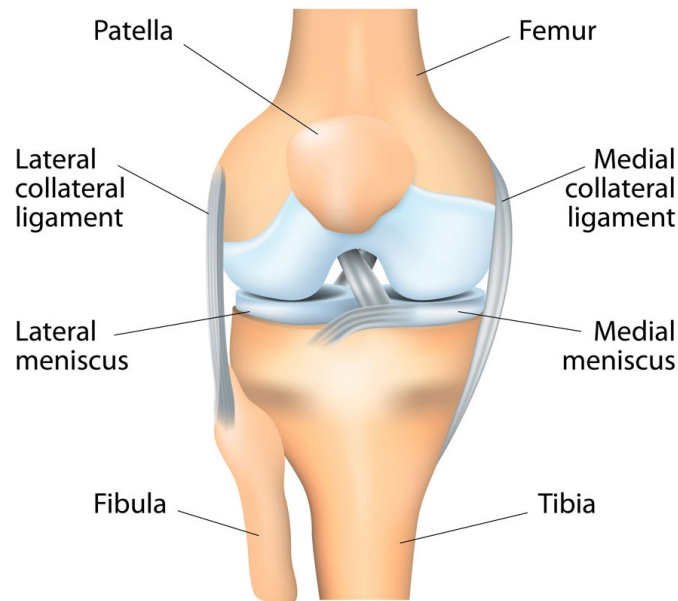


Figure 2.1: Anatomy of the human knee joint (patellar tendons/ligaments are not shown here for clarity) [22]

Figure 2.1 shows four ligaments, connecting the femur to the tibia. Lateral and medial collateral ligaments connect medial sides and lateral sides of the knee together, stabilizing the knee joint in the medial-lateral direction. Moreover, anterior and posterior cruciate ligaments prevent the sliding of femur and tibia in the anteroposterior direction [19,23]. There are two fibrocartilage structures located between femoral condyles and tibial plateaus, called menisci shown in the Figure 2.1. In addition to the stabilization of the knee joint, menisci have a significant role in a shock absorption and force distribution [21]. Knee joint capsule surrounding the knee joint is filled with the synovial fluid, which facilitates the cartilage lubrication and provides smooth sliding between femoral, tibial and patellar cartilages. The joint capsule supplies nutrition together with synovial fluid for joint cartilage [18].

Articular cartilage is a specific type of a connective tissue covering ends of articulating bones inside the synovial joints. Cartilage provides a smooth surface over bones with a very low friction coefficient and helps the knee joint to distribute the loads over the whole surface and dissipate the produced energy resulting from the knee joint loading [11,24,25].

2.2 Structure and composition of articular cartilage

Articular cartilage has no nerves and the only cell type inside cartilage is chondrocyte forming only about 1% of the human cartilage volume [24,26]. Chondrocytes are embedded within the extracellular matrix (ECM), and thus, their mobility inside the tissue is limited [1]. Furthermore, the metabolic activity of chondrocytes depends on the loading conditions of cartilage and they also synthesize macromolecules of cartilage [27,28].

The main constituents of articular cartilage are collagen fiber type II (50-80% of the dry weight and 15-22% of the wet weight of cartilage), proteoglycans (30% of the dry weight and 4-7% of the wet weight) and interstitial fluid (50-85% of cartilage wet weight) [11,29,30]. The aforementioned values can vary dramatically based on the individual, health status, cartilage site and joint location [4,31]. These constituents are arranged and distributed in a depth-wise manner modulating the depth-dependent stress and strain distribution inside the cartilage tissue [16,20].

2.2.1 Collagen network

Collagen fibers are structural proteins forming three polypeptide chains. They are the main component in connective tissues and the most abundant protein inside the human body [29]. Collagen fiber type II contains 90 to 95% of the whole collagenous network of articular cartilage [32]. The type II fibers form the main collagen network which is cross-linked together with *e.g.* type IX and XI collagen fibrils. The collagen network forms the main supportive structure in cartilage and also helps to restrict the movement of proteoglycans and interstitial fluid [11,33,34]. The collagen network has also an important role for cartilage mechanics due to the high tensile stiffness of collagen fibrils. Moreover, the collagen network architecture regulates the fluid pressure and flow direction [35,36].

Collagen network can be subdivided into three different zones, according to a depth-dependent orientation, architecture (Figure 2.2). The composition is highest in deepest zone and lowest in the superficial zone. In the superficial zone, collagen fibers are organized parallel to the surface of cartilage. This characteristic provides cartilage with its high tensile stiffness. By traversing deeper in the cartilage, collagen fibers start bending towards the vertical direction and are more randomly oriented. This area is called as the middle. In the deep zone, collagen fibers are oriented perpendicular to the subchondral bone and this zone provides the highest compressive force resistance of cartilage. The calcified cartilage zone connects cartilage to subchondral bone by anchoring the collagen fibers to the bone in perpendicular direction to the cartilage surface [24,37,38].

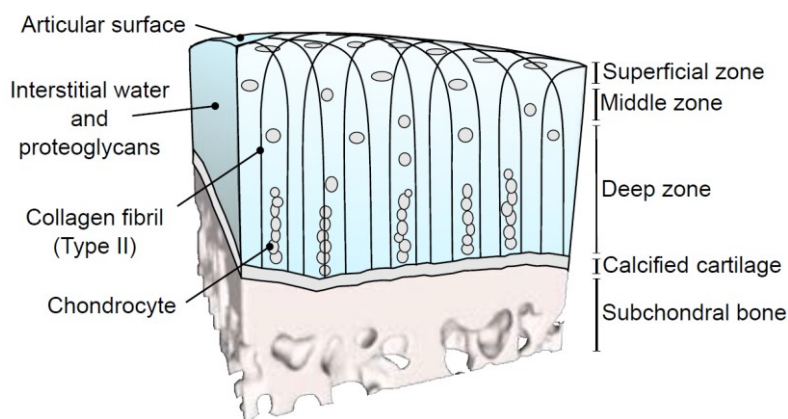


Figure 2.2: Illustration of the cartilage zones and main structures (from [39] with permission)

2.2.2 Proteoglycans

PGs are heavy, immobile macromolecule proteins, forming the second largest portion of cartilage organic materials. Core protein of the PG is attached through multiple branches to glycosaminoglycans (GAGs, Figure 2.3). There are two types of PGs existing in articular cartilage including large aggregated PG molecules and small PG molecules like fibromodulin. GAG chains possess a high negative charge causing repulsive forces between the chains [11,26]. The negatively charged PGs are able to attract the water inside the cartilage effectively, causing osmotic pressure difference and consequently leading to swelling of cartilage. Cartilage has a great load recovery property due to the osmotic swelling. The collagen network resists the osmotic swelling. This causes formation of pre-strain in the collagen fiber [40]. Collagen pre-strain substantially contributes to the compressive (and tensile) stiffness of cartilage [40,41].

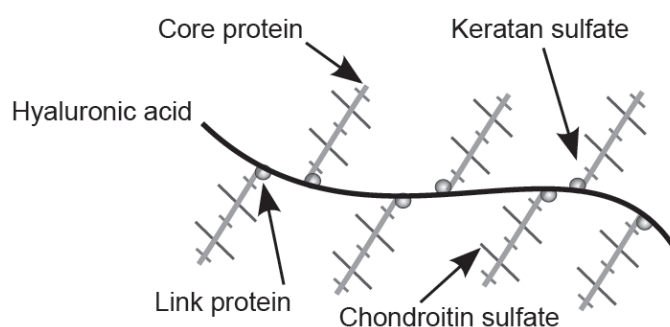


Figure 2.3: The structure of proteoglycan (From [42] with permission)

In common with collagen fibers, PGs are distributed in a depth-wise manner. The PG content is the lowest in the superficial zone while the PG content increases towards the deep zone where its content is the highest [11].

2.2.3 Interstitial fluid

The interstitial fluid in cartilage contains water, gas and metabolic products. Articular cartilage is a porous tissue. This enables fluid to flow inward to and outward from the tissue depending on tissue permeability. The fluid content of cartilage is also distributed in a depth-wise manner with the highest proportion in the superficial zone (80% of the tissue weight) and the lowest proportion in the deep zone (65% of the tissue weight) [24]. The collagen network and fluid matrix of cartilage have a significant role in mechanical response of cartilage during dynamic and impact loads. During these loads, the collagen network is in tension and consequently the collagen network contributes in tissue dynamic stiffness [43]. In addition, due to the relatively low cartilage permeability, the fluid pressurizes at high loading rates, thus the fluid pressurization can carry a large proportion of the total load [44]. When

cartilage is under prolonged loads, the interstitial fluid flows out, and the solid matrix is the main contributor to the tissue stiffness [11].

2.3 Mechanical properties of cartilage

Mechanical properties of cartilage vary a lot depending on species and location where cartilage tissue is located. Time-dependent poroelastic behavior of cartilage tissue can be roughly estimated by three independent material parameters including Poisson's ratio, Young's modulus or aggregate modulus at equilibrium and (hydraulic) permeability (Table 2.1). The Poisson's ratio is defined as the proportion of transverse strain to longitudinal strain (in the direction of applied load). The aggregate modulus (H_A , obtained from confined compression) is referred to tissue modulus at its equilibrium phase (*i.e.* when fluid flow has ceased) and (hydraulic) permeability (k_H) describes the ability of the tissue to allow a fluid to pass through it. Using the aggregate modulus and the Poisson's ratio, the cartilage Young's modulus can be derived. Cartilage possesses relatively low permeability (*e.g.* $3.66 (\pm 2.86) \times 10^{-15} \frac{\text{m}^4}{\text{Ns}}$ for human hip joint cartilage [45]). Due to this fact, an outflow of interstitial fluid is relatively slow even during fast compression generating time-dependent behavior of cartilage.

Under dynamic loading, like walking and other types of fast loadings, loading and strain-rates are high. The low permeability of the tissue prevents fast outflow of the interstitial fluid which causes fluid pressurization in the tissue enabling fluid matrix to carry over 80% of the total load of cartilage [44]. In addition, during dynamic loading the collagen network is put under tension at the superficial zone of cartilage. Thus, collagen fibrils also contribute to the dynamic stiffness of cartilage. Furthermore, collagen has intrinsic viscous properties meaning that collagen has different contribution to cartilage mechanics at different loading rates [46]. The amplitude of cartilage dynamic modulus remains almost unchanged at high strain rates, due to the fact that fluid has achieved its maximum potential of pressurization at higher frequencies [47,48], while small differences are most likely caused by the viscoelasticity of collagen fibers [46].

Under static compressive loading, the fluid flows slowly out of cartilage. This phenomenon is called tissue relaxation and its rapidness is mainly controlled by permeability but also by the viscoelasticity of collagen fibers. Following the relaxation (in compression), the fixed charged PGs in the ECM are forced closer to each other, resulting in an increasing repulsive electrostatic force. At the steady-state, the fluid flow has ceased and negatively charged PGs are the main constituent maintaining the stiffness of cartilage. Therefore, the equilibrium modulus of cartilage is mainly caused by the PGs. Furthermore, as the fluid is not anymore pressurized at the steady-state, the cartilage becomes softer [30,31,36,49].

Table 2.1: The material properties of cartilage in different species [37]. Data is averaged from lateral and medial femoral condyles and patellar groove.

	ν (-)	H_A (MPa)	$k_H \times 10^{-15} \left(\frac{m^4}{Ns}\right)$
Human	0.06	0.61	1.50
Bovine	0.34	0.76	0.77
Dog	0.26	0.69	0.84
Monkey	0.22	0.71	3.80
Rabbit	0.25	0.60	2.56

ν = Poisson's ratio, H_A = aggregate modulus, k_H = (hydraulic) permeability

In addition to the fact that mechanical behavior of cartilage is time-dependent, it is also different in a depth-wise manner according to the collagen fibers [50]. The directional tensile stiffness of the cartilage is associated with the collagen network orientation. As a result, the tensile stiffness is highest at the superficial zone and lowest at the deep zone near the subchondral bone. The ability of cartilage to resist shear and tension arises mainly from the collagen network orientation in the superficial and middle zone [24], while the deep zone also contribute to shear resistance partially [51].

2.4 Osteoarthritis and its effects on tissue structure

OA is a degenerative disease of articular cartilage and also the most prevalent joint disease, causing numerous disabilities and indirect deaths annually [52]. Idiopathic (*i.e.* primary) OA has no clear cause of onset of disease as it is often involved with ageing. While, post-traumatic OA (one form of secondary OA) develops following a joint trauma. Regarding the human body, OA can occur in different synovial joints, but the knee joint has been reported as the most prone joint for OA development [25]. As there are no nerves in the cartilage tissue, patients suffering from OA notice symptoms [53] (pain, joint stiffness) typically when cartilage tissue has almost completely been degenerated [54] (*i.e.* there is cartilage-on-bone or bone-on-bone contact in the knee joint). Immobilization, overweight and joint injury are well-known risk factors for the onset of OA. To prevent the onset and progression of OA, moderate regular exercises and weight loss are recommended [13,55]. Currently either primary or secondary OA cannot be cured [56]. However, there are some non-pharmacological treatments available like electrical stimulation and thermal therapies as well as physical rehabilitation that aim to slow down the progression of the disease and/or pain relief [55,57]. Ultimately, the disease progresses to the late stage in which the only treatment is a total joint replacement surgery [58].

From the structural point of view, the onset site of OA is not always clear. Some investigators have suggested that OA is initiated by the changes in the subchondral bone [59], and this might be the case in primary OA. However, it often starts from the superficial layer of cartilage by minor alteration of collagen and PG matrices, followed by the synthetic response of the chondrocytes at its middle stages, and finally ending by the decline of chondrocytic response for repairing the cartilage and progressive loss of cartilage volume [14,25,60,61]. At the early stages of OA, collagen network fibrillation and PG loss in the superficial zone of cartilage have been reported [14]. As the fibrillated collagen network is not capable of resisting against the swelling pressure caused by the negatively charged PGs, cartilage swells even more [62]. In addition, the fibrillation of the collagen network enables the PGs to escape from the ECM leading to PG loss [14,25,63]. Followed by the changes in the collagen network and PG content, chondrocytes start acting by releasing mediators (*i.e.* peptide and lipid mediators [64]) to stimulate the tissue. Further progression of OA results in alterations in collagen architecture and content reduction, as well as reduction in the PG content [14].

The Mankin and ICRS grading systems are well-established grading systems, often used for determining the stage of OA development [65]. For example, in ICRS grading, classification of cartilage ranges from fully intact cartilage (ICRS0) to partially degenerated cartilage (ICRS1-ICRS3) and finally to totally worn out cartilage (ICRS4) [66]. The scoring criterion is based on visual inspection using arthroscopy to evaluate the cartilage surface [3,67]. In contrast, Mankin grading is used for histological slices, showing more specific properties. While, it requires biopsy or *in vitro* samples [63].

2.5 Biomechanical characterization of articular cartilage

Biomechanical testing protocols are often designed depending on a physiological *in vivo* condition of the soft tissue. The tendons and ligaments are mainly under tensile loading in the body, and thus, a tensile test is usually used for determination of their biomechanical behavior [68]. In contrast, articular cartilage is in charge of providing smooth bearing surface under the compressive and shear forces and distributing the load. For that reason, a compression test is commonly used for characterization of articular cartilage [69].

Biomechanical behavior of cartilage varies a lot by subject. It also changes depending on a location of a joint in the body and depending on a location of cartilage tissue inside the joint (*e.g.* weight-bearing or non-weight-bearing location). The biomechanical response is also a depth-dependent. Therefore, different characterization methods, geometries and loading mods have been defined [24,70].

2.5.1 Mechanical testing configurations

There are three commonly used uniaxial testing configurations for articular cartilage. Confined and unconfined tests are performed to measure cartilage plug or explant compressive properties whereas an indentation test measures compressive properties of the articular cartilage attached to subchondral bone (also called as an osteochondral explant, Figure 2.4). In addition, tensile tests are performed to measure tensile properties of cartilage [69].

Unconfined and confined tests characterize the bulk properties of cartilage samples, while indentation test deals more with the local properties. In the unconfined compression test, impermeable plates are used for compressing the tissue, allowing the fluid to flow only in transversal direction. Impermeable confining chamber and porous filter are used for the confined compression test, where (vertical) fluid flow is possible only through the permeable filter. Lateral deformation in the confined test is prevented by the confining chamber. In the indentation test, cartilage is often compressed using a cylindrical plane-ended or a hemispherical indenter while the fluid flow is not restricted in any way [69,71] (Figure 2.4).

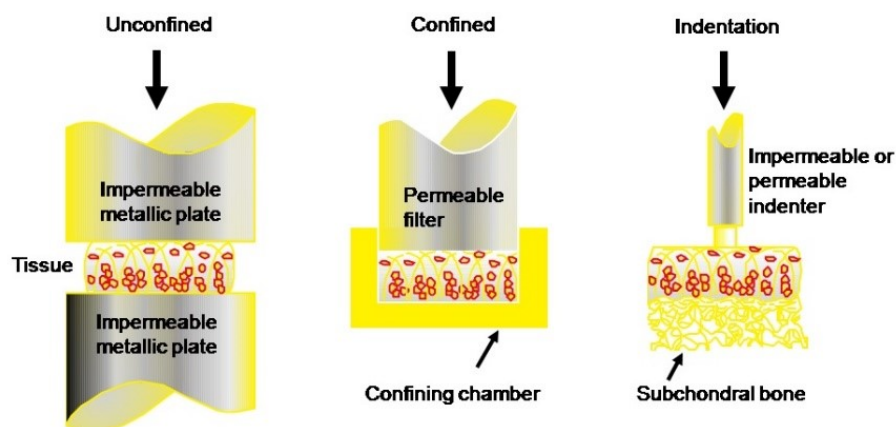


Figure 2.4: Typical biomechanical compression test configurations: unconfined, confined and indentation measurement geometries [72].

Tensile tests are used for studying the tensile behavior of the tissue. A tensile stress-relaxation or creep protocol (see more details about loading protocols from Section 2.5.2) is exerted to dumbbell-shaped cartilage specimen and resulting deformation (strain) or stress is recorded [50]. In an ultimate (tensile) test, the material is tested until a failure. This results in a stress-strain graph shown in the Figure 2.5. At the early steps of loading, the collagen fibers in cartilage are crimped. As they are progressively recruited, the stress-strain curve becomes initially nonlinear. This area is called as toe region. The linear region in the stress-strain curve, used for characterizing tensile elastic modulus, is related to the situation when all of the collagen fibers are straightened and contribute to carrying the load. Following the elastic

region, in the plastic region, permanent deformation is induced in the fibers (*i.e.* single bundles failure) until the catastrophic failure happens when all of the individual fibers fail [50,73].

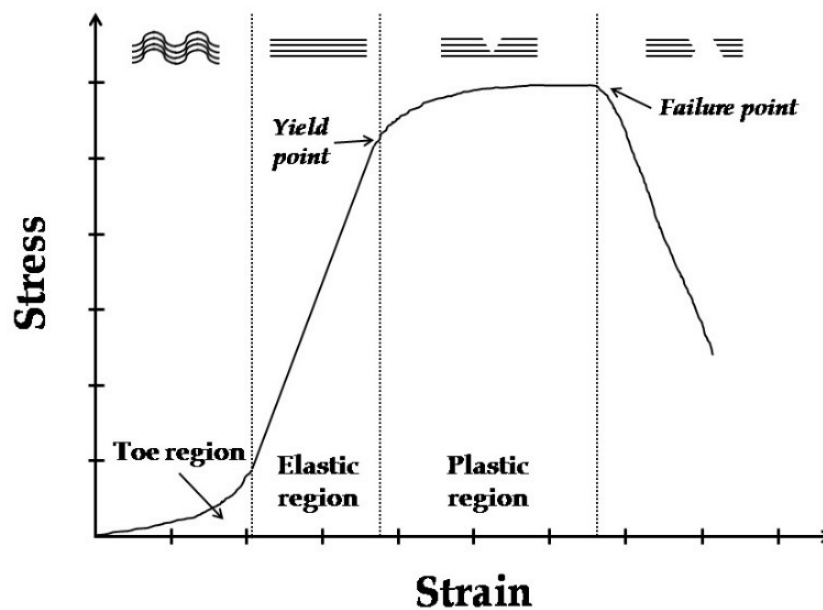


Figure 2.5: Representative stress-strain curve in an ultimate tensile test [72].

2.5.2 Loading protocols

Compressive and tensile properties of articular cartilage are tested via different loading protocols such as creep, stress-relaxation and dynamic loading. Different protocols aim to determine cartilage biomechanical properties including compressive and tension properties under different loading conditions [69]. Creep or stress-relaxation protocols aim to determine the viscoelastic properties of cartilage via stress- or strain-controlled loading, respectively. The dynamic test aim to determine dynamic properties like dynamic modulus and phase difference.

2.5.2.1 Creep

In the creep protocol, a constant load is applied fast and changes in a deformation are measured (Figure 2.6). The cartilage constituents, mainly the collagen fibers and pressurized interstitial fluid respond to the instantaneously applied load. Due to the extremely low permeability, the fluid cannot immediately flow freely out from the tissue and the fluid pressurizes in the cartilage. This is followed by the outflow of interstitial fluid. This fluid flow behavior causes time dependent deformation of cartilage until it reaches the equilibrium (steady-) state (*i.e.* no fluid flow) [8,73].

2.5.2.2 Stress-relaxation

In the stress-relaxation test, a constant displacement (strain) is applied and the resulting force is monitored (Figure 2.6). The relatively fast initial displacement results in pressurization of interstitial

fluid and tension in the collagen fibers. This can be observed as a peak force in the stress-relaxation force graph (Figure 2.6). Applied strain rate has a substantial effect on the peak force, a slow rate leads to a smaller peak force. As the time passes, the fluid starts flowing out of cartilage and redistributing, and as a consequence cartilage relaxes until it reaches the equilibrium (steady-)state [8,73].

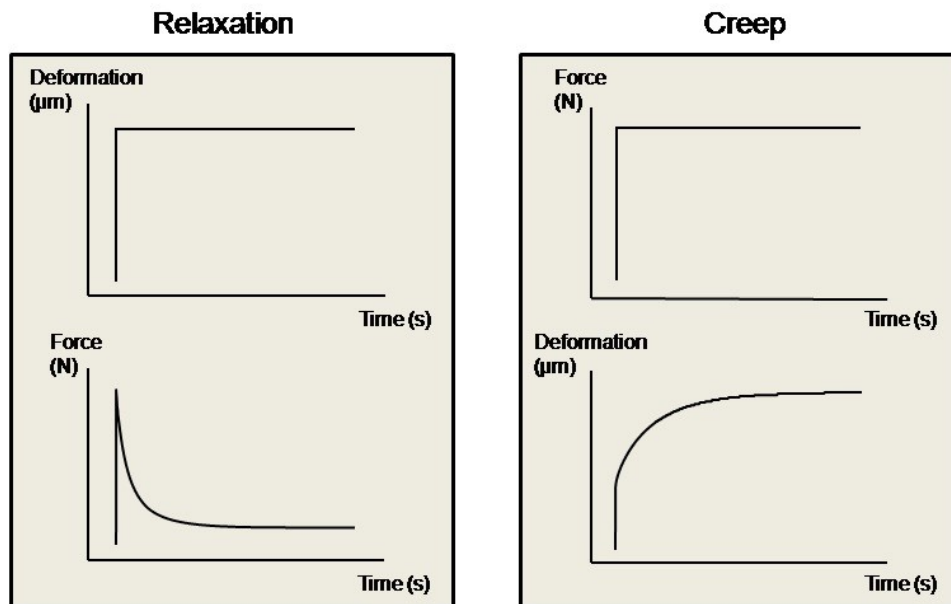


Figure 2.6: Deformation and force as a function of time in the (left) stress-relaxation and (right) creep protocols [72]

With regards to the equilibrium bulk properties of articular cartilage, cartilage is typically assumed to behave like a isotropic linear elastic material [8,69]. Therefore, the experimental data can be analyzed using Hooke's law as the equilibrium stiffness of cartilage is controlled by the solid matrix [15,16]. Through multiple steps of stress-relaxation with increasing strain at subsequent steps, one can measure the equilibrium stresses obtained at the end of each relaxation step and calculate the equilibrium modulus from the stress-strain slope using a linear least squares fit. The equilibrium (Young's) modulus is defined from Hooke's law as follows:

$$E_{eq} = \frac{\sigma}{\epsilon}, \quad (2.1)$$

where E_{eq} is the equilibrium modulus, σ is the stress and ϵ is the strain (at equilibrium).

As the strain field is not uniformly distributed on the top layer of cartilage when using indentation, Hayes et al. defined a mathematical solution based on theory of elasticity for obtaining the relation between the pressure applied by the indenter and the tissue modulus (*i.e.* equilibrium and dynamic moduli) assuming cartilage as infinite elastic layer and indenter as rigid axisymmetric punch with

different shapes [74]. When indentation test is used, based on the paper by Hayes et al., corrected (or true) equilibrium modulus is of a form:

$$E = \frac{(1 - \nu^2)\pi a}{2\kappa h} P, \quad (2.2)$$

where P is the indenter pressure, E is the corrected equilibrium or dynamic modulus, ν is the Poisson's ratio, a is the indenter radius, h is the sample thickness and κ is a non-dimensional constant (also called as Hayes correction factor) which depends on Poisson's ratio of a material and the aspect ratio of the sample (*i.e.* a/h).

2.5.2.3 Dynamic

Dynamic tests (*i.e.* repeated loading-unloading cycles) are applied to study the viscoelastic response of articular cartilage. In this type of a mechanical test, a sinusoidal stress or strain is applied and the resulting displacement or force is measured as a function of time [12]. The dynamic compression of articular cartilage characterizes primarily the tensile properties of the collagen network by exhibiting direct tension in the fibrils (especially in indentation) and by pressurization of the interstitial fluid which produces tensile stresses in the collagen fibers during alternating loading [73].

The dynamic modulus of a viscoelastic material has elastic and viscous proportions. The storage modulus is related to the energy stored in the material (*i.e.* reversible work) and the loss modulus is related to the amount of the energy dissipated by the material (*i.e.* irreversible work) [75]. The storage modulus E_{storage} and the loss modulus E_{loss} can be calculated from the dynamic sinusoidal test as:

$$E_{\text{storage}} = \frac{\sigma_0}{\varepsilon_0} \cos \delta, \quad (2.3)$$

$$E_{\text{loss}} = \frac{\sigma_0}{\varepsilon_0} \sin \delta, \quad (2.4)$$

where σ_0 is calculated from the peak-to-peak value of the stress and ε_0 is calculated from the peak-to-peak value of the strain, δ is the phase difference between the sinusoidal stress and strain curves. The dynamic modulus (E_{dyn}) is defined as:

$$E_{\text{dyn}} = \sqrt{E_{\text{loss}}^2 + E_{\text{storage}}^2}, \quad (2.5)$$

As in the case of the equilibrium modulus, the Hayes equation (eq. 2.2) must be used for obtaining the correct dynamic (or storage or loss) modulus if measurement is conducted in indentation geometry.

2.6 Computational modeling of articular cartilage

Computational modeling is a way of quantifying the physical quantities or mechanical parameters, which cannot be measured directly. Different material models for the highly nonlinear anisotropic articular cartilage have been introduced such as isotropic and transversely isotropic biphasic materials [76,77] and most recently the fibril-reinforced biphasic materials [15,16,40]. The latest material models (*i.e.* fibril-reinforced biphasic) were developed to capture the nonlinearities of the cartilage behavior by taking into account the depth-dependent inhomogeneities and representing the mechanical function of cartilage based on cartilage constituents (collagen, PGs and interstitial fluid) [78]. The advantage of the fibril-reinforced biphasic material model over the conventional biphasic model is that it takes collagen fibers into account, so the peak response is more accurately estimated [15].

2.6.1 Isotropic and transversely isotropic linear elastic materials

The simplest way of describing the mechanical behavior of a material is to assume similar mechanical properties in each direction. This kind of material is called as isotropic material. Generalized Hooke's law defines isotropic linear elastic relationship between stress and strain as (using Voigt notation):

$$\begin{bmatrix} \sigma_{11} \\ \sigma_{22} \\ \sigma_{33} \\ \sigma_{12} \\ \sigma_{13} \\ \sigma_{23} \end{bmatrix} = \mathbf{C}^E \begin{bmatrix} \varepsilon_{11} \\ \varepsilon_{22} \\ \varepsilon_{33} \\ \varepsilon_{12} \\ \varepsilon_{13} \\ \varepsilon_{23} \end{bmatrix}, \quad (2.6)$$

where σ_{ii} and ε_{ii} are the stresses and strains aligned on the direction of basis axes, and σ_{ij} and ε_{ij} are shear components. Note that the shear stresses and strains are symmetric (*i.e.* $\sigma_{ij} = \sigma_{ji}$ and $\varepsilon_{ij} = \varepsilon_{ji}$). \mathbf{C}^E is the stiffness matrix described as:

$$\mathbf{C}^E = \frac{E}{(1+\nu)(1-2\nu)} \begin{bmatrix} 1-\nu & \nu & \nu & 0 & 0 & 0 \\ \nu & 1-\nu & \nu & 0 & 0 & 0 \\ \nu & \nu & 1-\nu & 0 & 0 & 0 \\ 0 & 0 & 0 & 1-2\nu & 0 & 0 \\ 0 & 0 & 0 & 0 & 1-2\nu & 0 \\ 0 & 0 & 0 & 0 & 0 & 1-2\nu \end{bmatrix}, \quad (2.7)$$

To model a material behavior of a biological tissue like meniscus, transversely isotropic linear elastic materials have shown to provide better results over the isotropic linear elastic material [79,80]. The transversely isotropic material behavior is described in two different planes; a plane of isotropy, where the mechanical properties in the plane are similar, and an orthogonal transverse plane, where the mechanical properties are different than in the plane of isotropy. Assuming the plane 1-2 as the plane of isotropy, the stiffness matrix is defined as:

$$\mathbf{C}^E = \begin{bmatrix} \frac{1}{E_{11}} & -\frac{\nu_{21}}{E_{22}} & -\frac{\nu_{21}}{E_{33}} & 0 & 0 & 0 \\ -\frac{\nu_{12}}{E_{11}} & \frac{1}{E_{22}} & -\frac{\nu_{32}}{E_{11}} & 0 & 0 & 0 \\ -\frac{\nu_{13}}{E_{11}} & -\frac{\nu_{23}}{E_2} & \frac{1}{E_{33}} & 0 & 0 & 0 \\ 0 & 0 & 0 & \frac{1}{G_{23}} & 0 & 0 \\ 0 & 0 & 0 & 0 & \frac{1}{G_{13}} & 0 \\ 0 & 0 & 0 & 0 & 0 & \frac{1}{G_{12}} \end{bmatrix}, \quad (2.8)$$

where E_{ij} is the Young's modulus in the direction ij , G_{ij} is the shear modulus in the direction ij and ν_{ij} is the Poisson's ratio in the direction ij .

2.6.2 Biphasic materials

The solid and the fluid matrices are defined separately in the biphasic theory. The solid matrix is often assumed as incompressible medium with no energy loss. The fluid dissipates the energy in the material. The stress tensors induced by solid and fluid matrices are [8,77]:

$$\boldsymbol{\sigma}_s = -n_s p \mathbf{I} + \boldsymbol{\sigma}_{\text{eff}}, \quad (2.9)$$

$$\boldsymbol{\sigma}_{\text{fl}} = -n_{\text{fl}}p\mathbf{I}, \quad (2.10)$$

where n_{s} and n_{fl} are relative solid and fluid volume fractions respectively, p is the fluid pressure and $\boldsymbol{\sigma}_{\text{eff}}$ is the effective solid matrix stress tensor. Accordingly, the total stress tensor is described as:

$$\boldsymbol{\sigma}_{\text{tot}} = \boldsymbol{\sigma}_{\text{s}} + \boldsymbol{\sigma}_{\text{fl}} = \boldsymbol{\sigma}_{\text{eff}} - p\mathbf{I}, \quad (2.11)$$

Darcy's law [81] is employed to describe the fluid flow:

$$q = -k\nabla p, \quad (2.12)$$

where q is the rate of the fluid flow, k is the (hydraulic) permeability of the material and ∇p is the (fluid) pressure gradient. Darcy's law is valid only with laminar and low velocity flows, which is true in most biological tissues [82]. The void ratio in the porous material is defined as the proportion of the fluid volume to the solid volume.

$$e = \frac{n_{\text{fl}}}{n_{\text{s}}}, \quad (2.13)$$

The deformation in the porous materials causes change in the void ratio, and consequently, changes in the permeability, which is described as [16,83] :

$$k = k_0 \left(\frac{1+e}{1+e_0} \right)^M, \quad (2.14)$$

where k , k_0 and e , e_0 are the current and initial values for the permeability and void ratio, respectively, and M is a constant describing the void-ratio-dependent factor of permeability [15].

2.6.3 Fibril-reinforced biphasic and poroelastic materials

The fibril-reinforced biphasic material is also composed of solid and fluid matrices. The solid matrix includes fibrillar collagen matrix as well as non-fibrillar porous PG matrix [15]. Moreover, as in the regular biphasic material, the fluid flow defines the time dependent behavior of the material [8].

The pores are continuously distributed in the solid matrix of poroelastic material models [84]. Whereas, there is a continuous distribution of solid and fluid phases in the biphasic material model [8]. Although they have implemented different formulations to model the soft tissue materials behavior, they are equivalent theories and give similar results [85]. Thus, in this thesis, biphasic and poroelastic terms are used together.

The collagen fibers have been modeled using different material behaviors such as linear elastic, nonlinear elastic or viscoelastic models [16,17,40,86], whereas the non-fibrillar matrix has been modeled widely using a Hookean or Neo-Hookean material model [40]. The inherent inhomogeneities of articular cartilage can also be taken into account by the implemented depth-dependent and/or spatial distribution of cartilage constituents into the material model [78].

The total stress tensor $\boldsymbol{\sigma}^t$ is defined as the stress caused by fibrillar and non-fibrillar matrices in addition to (pore) fluid pressure [16].

$$\boldsymbol{\sigma}^t = \boldsymbol{\sigma}_{nf} + \boldsymbol{\sigma}_f - p\mathbf{I}, \quad (2.15)$$

where $\boldsymbol{\sigma}_{nf}$ is the stress in the non-fibrillar matrix, $\boldsymbol{\sigma}_f$ is the stress in the fibrillar matrix and p is the fluid pressure.

2.6.3.1 Non-fibrillar matrix

The Hooke's law is valid only for strains less than 5%, while in the cartilage the typical strains caused by the physiological loads may exceed 5% [38,87]. Thus, the non-fibrillar matrix is modeled as a Neo-Hookean hyperelastic material, by which the non-fibrillar matrix stress ($\boldsymbol{\sigma}_{nf}$) is [40]:

$$\boldsymbol{\sigma}_{nf} = K \frac{\ln(J)}{J} \mathbf{I} + \frac{G}{J} \left(\mathbf{F} \cdot \mathbf{F}^T - J^{\frac{2}{3}} \mathbf{I} \right), \quad (2.16)$$

where G and K are the shear and bulk moduli (of the non-fibrillar matrix), respectively, \mathbf{F} is the deformation gradient tensor and J is determinant of the deformation tensor; $J = \det(\mathbf{F})$. Note that this formulation allows the material to be compressible.

Assuming infinitesimal strain in the non-fibrillar matrix, bulk and shear moduli can be expressed as a functions of the non-fibrillar matrix Young's modulus (E_{nf}) and Poisson's ratio (ν_{nf}):

$$K = \frac{E_{nf}}{3(1 - 2\nu_{nf})}, \quad (2.17)$$

$$G = \frac{E_{nf}}{2(1 + \nu_{nf})}, \quad (2.18)$$

The fluid flow in biphasic materials is also modeled according to the Darcy's Law (eq. 2.12) and the void-ratio-dependent permeability (eq. 2.14).

2.6.3.2 Fibrillar matrix

In the fibrillar matrix, collagen fibers can be implemented to the model either homogenously or in a depth-wise manner [15,88]. To model the collagen fibers, two categories of fibers are defined in the model; primary and secondary fibrils. The primary fibrils are organized according to the typical architecture of the collagen network. In the superficial zone, the fibrils are modeled parallel to the cartilage surface, in the middle zone the fibers bend towards the perpendicular direction and in the deep zone they are modeled perpendicular to the subchondral bone. Figure 2.7 depicts the natural distribution of the collagen fibers and an example of the modeled collagen orientation. The secondary fibrils are randomly oriented fibers, aiming to mimic the cross-links and random organization of the collagen network [16,83]. The stress tensor of primary ($\sigma_{f,p}$) and secondary ($\sigma_{f,s}$) fibrils can be written as [16]:

$$\sigma_{f,p} = \rho_z C \sigma_f, \quad (2.20)$$

$$\sigma_{f,s} = \rho_z \sigma_f, \quad (2.21)$$

where C is the fraction of the primary fibrils to the secondary fibrils, ρ_z is the depth-dependent collagen fraction. The total stress induced by the primary and secondary fibrils is [16]:

$$\sigma_f = \sum_{i=1}^{f_{tot}} \sigma_f^i, \quad (2.22)$$

where f_{tot} represents the total number of individual fibers and σ_f^i is the stress in an individual fiber.

There are several methods to model the mechanical behavior collagen fibers in the fibril-reinforced materials. The fibril modulus can be implemented constant and independent of the strain [15,16,89],

linearly increasing as a function of strain [90], exponentially increasing as a function of strain [91] or viscoelastic [16,45]. The linear relationship between the stress and strain in the collagen fiber result in a constant value of the collagen fibers modulus which is independent of the strain. In this model, the fibril stress (σ_f) and the Young's modulus of the fibrillar network (E_f) are:

$$\sigma_f = E_f \varepsilon_f, \quad (2.23)$$

where ε_f is the fibril strain. Naturally, the constant fibril modulus is not capable of modeling the nonlinearities of collagen fibers [92], if those are present. In that case, non-constant modulus (e.g. strain-dependent) can be considered.

Although nonlinear second and third order polynomial representations for the moduli of the collagen network have demonstrated the highest correspondence with the experimentally obtained measurements [92], the linear (*i.e.* first order polynomial) strain-dependent modulus has also showed good match with the experimental measurements in articular cartilage. On the other hand, the physical meaning of nonlinear moduli is difficult to interpret [90]. The (linear) strain-dependent collagen network modulus (E_f) can be defined as follows:

$$E_f = \frac{d\sigma_f}{d\varepsilon_f} = E_f^\varepsilon \varepsilon_f + E_f^0, \quad (2.24)$$

where E_f^0 is the initial fibril network modulus and E_f^ε is the strain-dependent fibril network modulus.

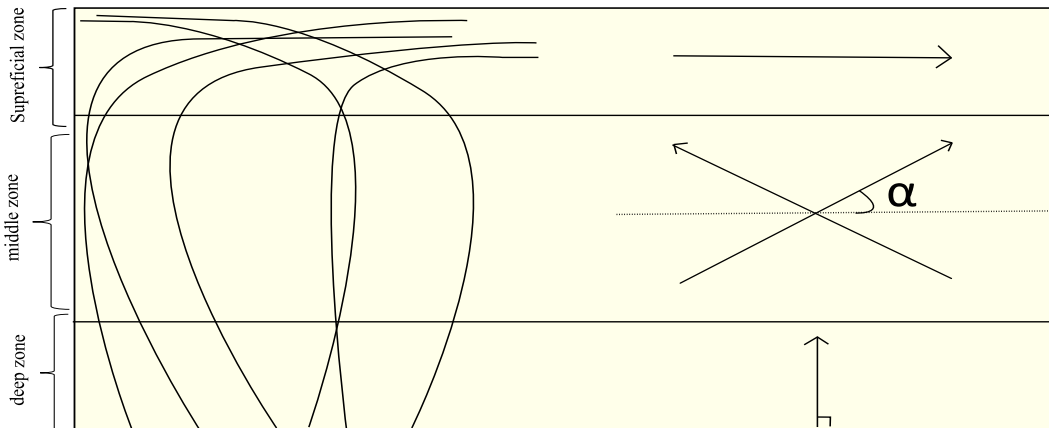


Figure 2.7: Typical “Benninghoff” type [93] collagen fiber architecture (left hand side) and schematic representation of computational representation of the collagen orientation in a fibril-reinforced material model (right hand side)

2.7 Optimization of the material parameters

In order to obtain material parameters, the parameters can be either measured directly or, if that is not possible, they can be obtained through combination of computational simulations and optimization. One way for obtaining material properties through optimization is to minimize the objective function ($\delta\bar{F}$) generated from normalized mean squared error between the simulation and the experimental data [89,94]:

$$\delta\bar{F} = \frac{1}{n} \sum_{i=1}^n \left(\frac{F_i^{\text{sim}} - F_i^{\text{exp}}}{F_i^{\text{exp}}} \right)^2, \quad (2.25)$$

where F_i^{sim} and F_i^{exp} are the simulated and experimental values (e.g. force), respectively.

For example, in the FRPE material with the strain-dependent collagen network modulus, one should optimize the initial and strain-dependent fibril network moduli, initial permeability and its strain-dependency factor in addition to the non-fibrillar matrix modulus (Figure 2.8).

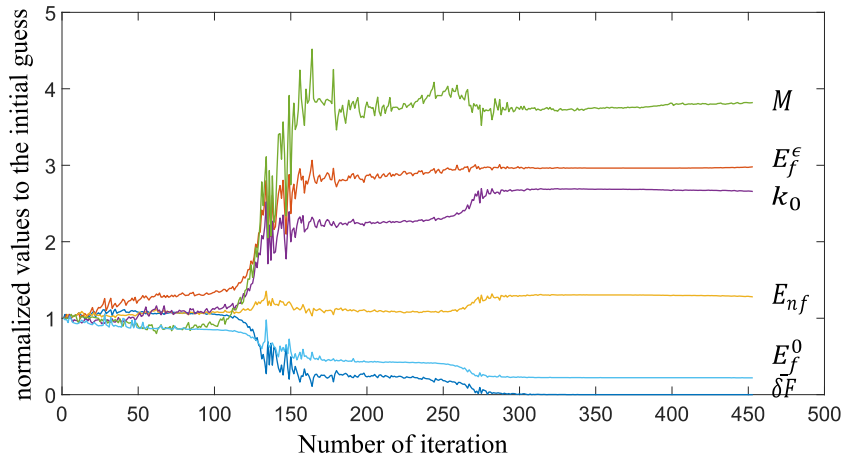


Figure 2.8: Representation of evolution of parameters optimizations

In the stress-relaxation measurements, the duration of compressive ramp is much shorter compared to the relaxation phase (less than a second compared to several minutes). As a result, there are more measurement data points in the equilibrium phase compared to the data points around the load peaks and the optimization error function value is more dependent to the relaxation phase error. To overcome this, the optimization routine can be focused on specific data points. For instance, a weighting factor can be used for weighting the peak forces in the objective function. Thus, the objective function is more sensitive to variations of the peak force [94]. The objective function value can be rewritten as follows in terms of normalized mean square error [94]:

$$\delta\bar{F} = \frac{1}{n} \sum_{i=1}^n \left(\frac{F_i^{\text{sim}} - F_i^{\text{exp}}}{F_i^{\text{exp}}} \right)^2 + w \frac{1}{m} \sum_{i=1}^m \left(\frac{F_{i,p}^{\text{sim}} - F_{i,p}^{\text{exp}}}{F_{i,p}^{\text{exp}}} \right)^2, \quad (2.26)$$

where $F_{i,p}^{\text{sim}}$ and $F_{i,p}^{\text{exp}}$ are the peak force values obtained from simulation and experiment and w is a weighting factor.

For parameter optimization, different nonlinear optimization tools can be used. One powerful tool is a minimum search algorithm (*fminsearch* function) implemented in Matlab software (V7.10.0, The MathWorks, Inc., Natick, MA). This function uses the Nelder-Mead simplex algorithm to optimize multiple variables in the nonlinear problems [68]. The algorithm produces n -dimensional vector around the initial guess by adding 5% of each component to its initial value. Following that, the algorithm modifies the values repeatedly by evaluation of the objective function. The algorithm evaluates the objective function value and the absolute changes in the parameters at each iteration. When the absolute objective function value and parameter differences between two consecutive iteration reaches the criteria, the optimization routine terminates.

There are some advantages and drawbacks associated with the Nelder-Mead simplex algorithm. It is a powerful tool for optimization, because it considers trial and error approach to find the optimized values and the method does not use numerical or analytic gradients [95]. In contrast, the main drawback is that it may converge to local minima. In order to ensure the uniqueness of optimized values and to avoid the local minima, the optimization routine can be repeated with slightly different initial guesses for initial values (*e.g.* different compared to initial guess or optimized values) to find out if the parameters represent the global minimum [94].

Chapter 3

Materials and methods

3.1 Sample preparation

The articular cartilage samples used in the current study were harvested from cadaver human knee joints by orthopedist at Kuopio University Hospital. During harvesting, all joints surfaces were ICRS-scored by same orthopedist. The process and use of the human tissue were approved by the National Authority for Medicolegal Affairs and the ethical committee of North-Savo hospital district, ethical permission number 134/13.02.00/2015.

Cylindrical intact osteochondral samples with 4 millimeters in diameter (Figure 3.1) were cut from medial, lateral, anterior and posterior sites of each tibia ($n = 27$). Afterwards, the samples were kept moist and immersed in Phosphate Buffered Saline (PBS, pH 7.4) with enzymatic inhibitor upon the preparation processes. The samples were then stored at $-23\text{ }^{\circ}\text{C}$ in sealed containers. Prior to a biomechanical indentation test, the samples were thawed at the room temperature for approximately 15 minutes.



Figure 3.1: Osteochondral sample under the optical microscope.

The sample thickness was measured using optical microscope (Zeiss, STEMI, SV8, Germany) with magnification of 1.6 times from 4 different quarters around the sample plug (from cartilage surface to the bone, perpendicular to the surface), and the mean value was calculated for the sample thickness. Figure 3.1 depicts one of the samples under the microscope.

3.2 Biomechanical indentation test

The biomechanical tests were carried out using indentation device for the osteochondral samples. The indentation device was a custom-made high-precision linear servo-motorized material testing device (Newport PM500-C Precision Motion Controller, Newport PM1A1798 Actuator, Irvine, CA, USA) with 250 g load cell to measure the load (Honeywell Model 31/AL311BL, Columbus, OH, USA). The diameter of the cylindrical plane-ended indenter (730 μm) was measured by the conventional optical microscope (6 \times magnification).

Prior to the indentation measurement, the bone end was flattened using sandpapers (Mirox P80, Mirka Oy, Uusikaarlepyy, Finland) and then glued to the bottom surface of a custom-made chamber. The chamber was then filled with PBS and enzymatic inhibitors (Figure 3.2). Perpendicularity of the indenter with respect to the sample surface was confirmed by naked eye from different directions and the adjustment was done if needed. In order to ensure a reliable contact of the indenter and the sample, 12.5 KPa (5 Newton) pre-stress was applied [89].

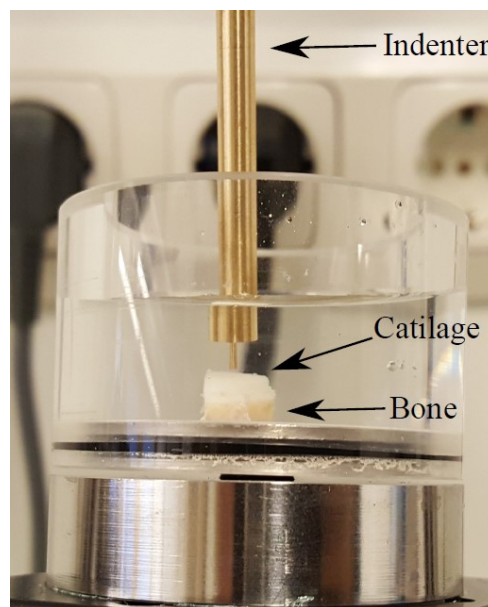


Figure 3.2: The experimental set-up

To measure the biomechanical behavior of cartilage, 4-step stress-relaxation protocol was defined. Each step consisted of 5% strain (of the remaining cartilage thickness) followed by a relaxation step of 15 minutes (Figure 3.3). In order to reach the predefined strain level, a ramp with a strain rate of 100%/s was applied [45,89,96].

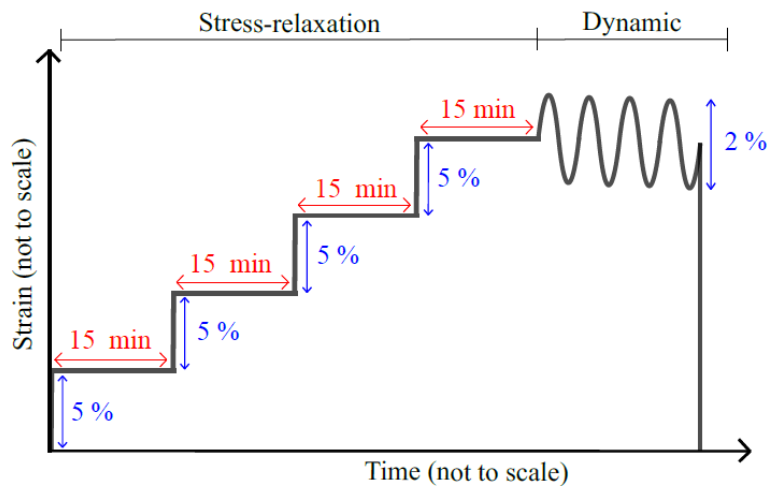


Figure 3.3: The stress-relaxation protocol in indentation followed by the dynamic protocol used in this study.

At the end of the final relaxation step (strain level at 20%), the dynamic sinusoidal test was carried out using 2% of the remaining thickness with frequencies of 0.005, 0.05, 0.1, 0.25, 0.5, 0.625, 0.833, 1, and 2 Hz (Figure 3.3).

3.2.1 Stress relaxation data preprocessing

The raw data from the stress-relaxation measurement was preprocessed for finite element modeling. Matlab software (V7.10.0, The MathWorks, Inc., Natick, MA) was used for data extraction and filtering the data. Prior to any further processing, Matlab (customized *getCursorInfo* function) was employed to manually select all peak and equilibrium force values from the curve. Afterwards, the raw data was smoothed and filtered using a moving average filter (window size of 100, pole at 1 and 100-folded zeros at 0.01) using *filtfilt* function to remove time lag (Figure 3.4). Each step data was extracted and saved for further analysis separately.

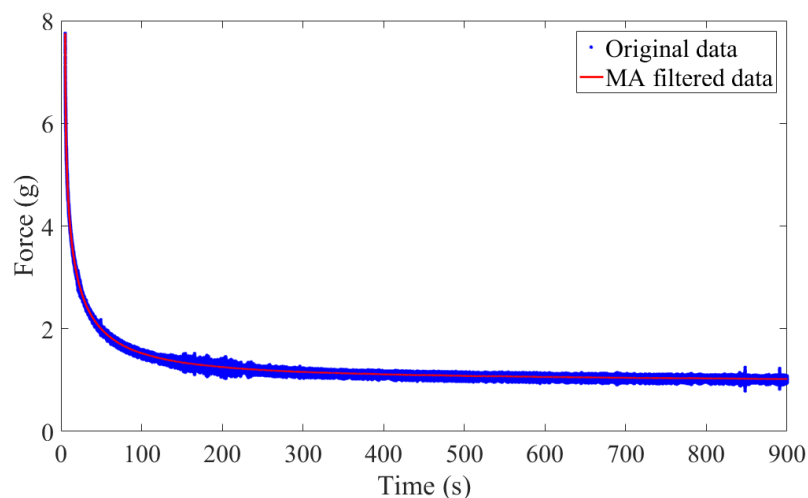


Figure 3.4: Original and moving average (MA) filtered data from a single step of stress-relaxation protocol.

3.2.2 Equilibrium modulus acquisition

Followed by the data preprocessing, the equilibrium moduli were calculated for the samples from the stress-relaxation data. First, the equilibrium force values were manually selected from the data (Figure 3.5).

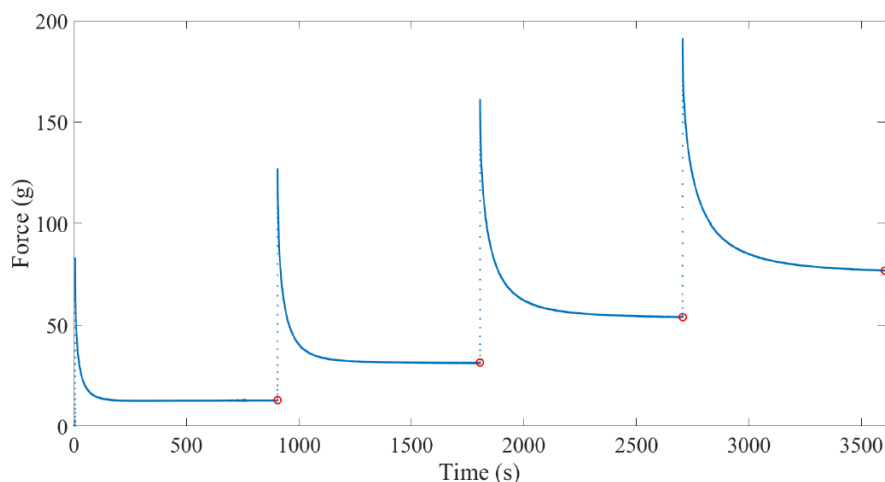


Figure 3.5: Example of the stress-relaxation data and selection of the equilibrium force points.

Then, the equilibrium stress at equilibrium point was calculated based on the indenter diameter. Considering strain level at each step, a general linear least-squares based fitting was used for acquiring the equilibrium modulus of the sample (*i.e.* calculated from the slope of the fitted line, Figure 3.6). The calculated equilibrium modulus was corrected using the Hayes correction factor (eq. 2.2) which considers the effects of the indenter size and sample thickness in an indentation geometry. The Poisson's ratio for the analysis was set to 0.4 [97].

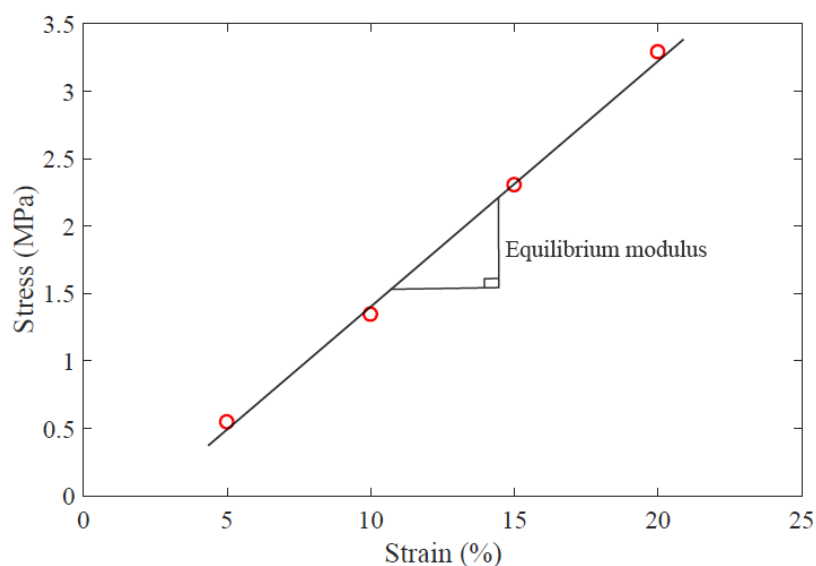


Figure 3.6: The uncorrected equilibrium modulus calculated from the linear least squares fit of the stress-strain data

$$\text{Stress}[\text{MPa}] = 0.18 \left[\frac{\text{MPa}}{\%} \right] \times \varepsilon [\%] - 0.03[\text{MPa}]$$

3.3 Dynamic tests data analysis

In order to calculate the dynamic modulus of the samples at different frequencies, the peak-to-peak values of forces and displacements were evaluated from the sinusoidal dynamic measurement data. A single term sinusoidal fit was utilized for both displacement and force data using *fft* function in Matlab (Figure 3.7). Following that, the amplitude of peak-to-peak forces and displacements obtained from the sinusoidal fit were extracted from each cycle and averaged over 4 cycles.

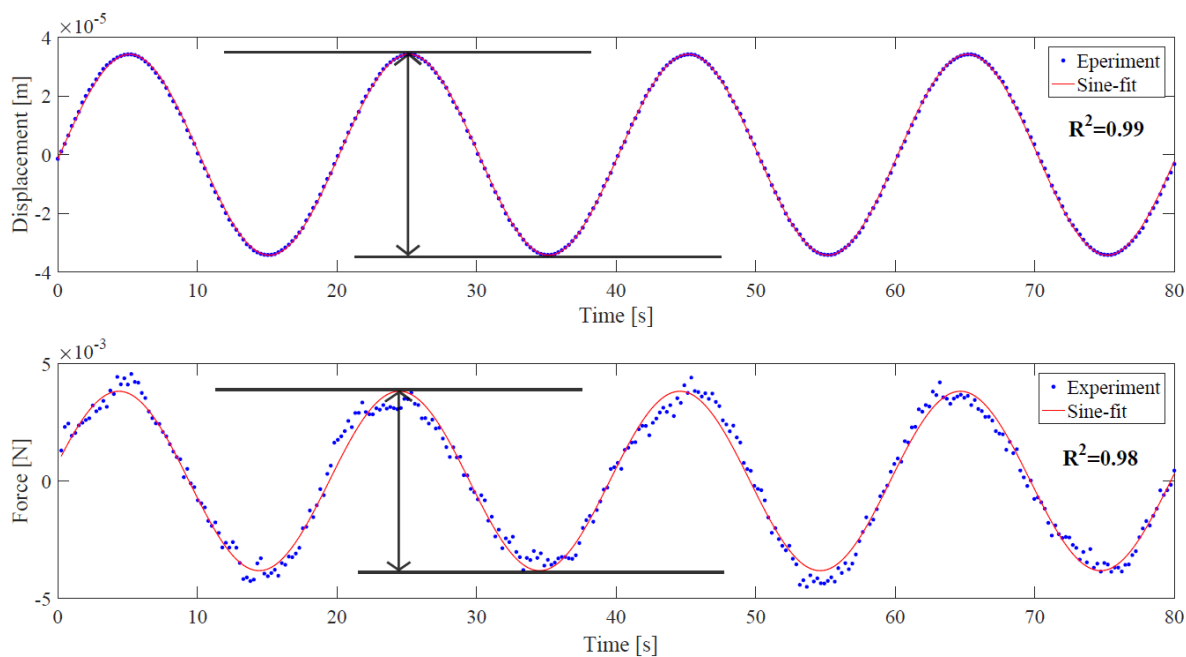


Figure 3.7: Experimental data from a dynamic sinusoidal test (0.05 Hz) and the fitted sinusoidal curves
 (Force = 3.4×10^{-5} [N] $\sin(0.31 \frac{1}{[s]} \times t [s] + 0.01)$, Displacement = 4.1×10^{-3} [m] $\sin(0.32 \frac{1}{[s]} \times t [s] - 0.04)$).

The phase shift was calculated from the frequency content of raw data. Fast Fourier transform (*fft* function in Matlab) was used for calculating the phase of each curve. The subtraction of the displacement phase angle and the force phase angle was considered as the phase shift. Figure 3.8 illustrates the frequency spectrum of one of the sample, calculated from the force data. As can be seen from the figure, the highest power amplitude is at 0.05 Hz, approximately. The insertion magnifies the spectrum around the peak for clarity.

The storage modulus (eq. 2.3) and loss modulus (eq. 2.4) were calculated from amplitudes of peak-to-peak forces and displacements together with sample thickness and the cross sectional area of the indenter. Subsequently, the dynamic modulus at each frequency was calculated. The effects of sample thickness and the indenter size were also taken into account by applying the Hayes correction (Eq. 2.2). The samples were assumed incompressible ($\nu = 0.5$) in the dynamic tests [98].

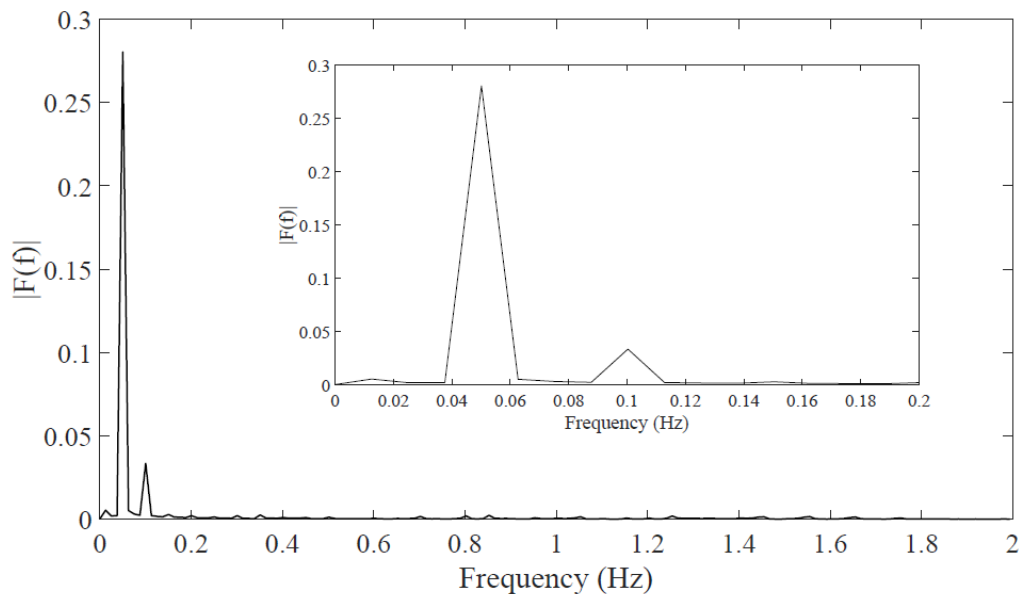


Figure 3.8: Frequency spectrum of dynamic force data (at 0.05 Hz), insertion magnifies the power spectrum around the peak

3.4 Finite element analysis

The sample-specific axisymmetric models were constructed in Abaqus finite-element software (V6.14, Dassault Systèmes Simulia Corp., Providence, RI). The samples were considered axisymmetric and the indenter was modeled as an analytic rigid surface with a rounded corner of $10\ \mu\text{m}$ in radius (*i.e.* a fillet, approximated from a microscopic image of the indenter, Figure 3.9). Depending of sample specific geometry (*i.e.* thickness = 2.98 ± 0.75 , more details can be found in appendix A), the samples were meshed by 225 to 600 linear axisymmetric pore pressure continuum elements (element type CAX4P).

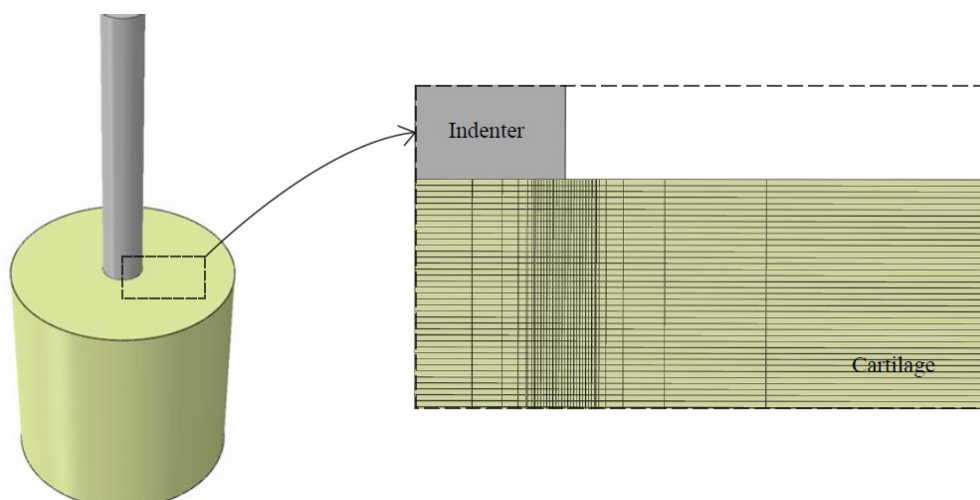


Figure 3.9: An example of a finite element model (extruded for clarity) and mesh of a sample.

The contact between the bottom of the indenter and cartilage surface was modeled as displacement boundary condition for computational efficacy. The contact between the lateral edge of the indenter and

cartilage surface was modeled using a frictionless hard contact (both in normal and tangential direction with no separation option) to prevent folding of the cartilage mesh. The displacement of the symmetry axis was fixed in a lateral direction (symmetry boundary condition) while the bottom of the cartilage mesh was fixed in the axial direction. Free fluid flow (zero pore pressure) boundary condition was applied to the free surfaces, while the contact surface between the cartilage mesh and the indenter was sealed [89].

The fibril-reinforced poroelastic material model (eq. 2.15) was applied to the cartilage. The collagen network was modeled with 4 organized collagen fibers (primary fibrils) and 13 randomly oriented fibrils (secondary fibrils) [16]. The fibril network architecture was modeled parallel to surface homogeneously throughout the tissue depth because there was no information regarding the collagen architecture and thickness of each cartilage zone. It is obvious that during the latest steps of stress-relaxation (15-20% of strain) middle and deep layers of cartilage might start affecting the results. However, the detailed implementation of zonal structure also affects to the optimization results, and by assuming homogeneous structure, the optimization results will be independent of the collagen structure. The ratio of the primary fibrils density to secondary fibrils density was based on literature ($C = 12.16$, see eq. 2.20) [83,89]. The strain dependent fibril modulus was used for modeling the nonlinear mechanical behavior of the collagen fibril network (Eq. 2.26). The non-fibrillar matrix was modeled as porohyperelastic Neo-Hookean material (Eq. 2.16, $\nu_{nf} = 0.42$ [89]). Permeability was assumed to be void ratio- (*i.e.* deformation-) dependent (Eq. 2.19, $e_0 = 3$ [72] *i.e.* $n_{fl} = 0.75$ and $n_s = 0.25$, respectively).

Soils consolidation analysis with implicit time integration was used for solving time-dependent coupled pore fluid diffusion and stress analysis in Abaqus (v6.14). The maximum allowed pore pressure change per increment was set to 1 MPa. The reaction force output was recorded from the reference point of the indenter (used for controlling both displacement boundary condition and the edge (contact surface) of the indenter).

3.5 Material parameter optimization

In spite of applying pre-stress to ensure the contact in the experiments, the contact of the sample and the indenter was not necessarily perfect in the initial step of stress-relaxation. One possible reason for this could be a rough cartilage surface causing a detection of an initial force even though the indenter is not yet in perfect contact. On the other hand, when the material parameters are optimized using more than two steps of stress-relaxation, the high nonlinearities arisen from the inherent inhomogeneities of cartilage may become dominant. This often leads to a poor optimization performance and coefficient of determination (R^2 value). For those reasons, only the second and the third steps of stress-relaxation were considered in the optimization process.

The Matlab optimization routine *fminsearch* was utilized to find the minimum of the modified mean squared error (eq. 2.28) of the simulated and experimental data. The weighting factor value ($w = 1$) was based on preliminary analyses, and hence, the objective function for the *fminsearch* routine was:

$$\delta\bar{F} = \frac{1}{n} \sum_{i=1}^n \left(\frac{F_i^{\text{sim}} - F_i^{\text{exp}}}{F_i^{\text{exp}}} \right)^2 + 1 \times \frac{1}{2} \sum_{i=1}^2 \left(\frac{F_{i,p}^{\text{sim}} - F_{i,p}^{\text{exp}}}{F_{i,p}^{\text{exp}}} \right)^2 \quad (3.1)$$

The optimized values were the initial fibril network modulus (E_f^0), the strain-dependent fibril network modulus (E_f^ε), the non-fibrillar matrix modulus (E_{nf}), the initial permeability (k_0) and the permeability strain-dependent coefficient (M). In order to ensure the uniqueness of the optimized values (*i.e.* to find global minimum), a parametric sensitivity analysis was conducted. The optimized values of nine randomly chosen samples were altered by 10% and the optimization process was conducted once again to confirm the global minimum [94].

3.6 Data analysis

In order to establish the relationships of OA progression and biomechanical properties of the samples, they were grouped using two different approaches. The first grouping was based on visual ICRS scoring of cartilage quality and the second grouping was based on the equilibrium modulus of the samples (*i.e.* biomechanical grouping).

3.6.1 ICRS (visual inspection-based) grouping

The ICRS system for cartilage grading was used for evaluating the possible development of OA [66]. The ICRS scoring is based on the visual inspection. The scoring deals with assessment of the region of interest surface of the cartilage via arthroscopy. Expert orthopedist evaluated cadavers' cartilage surface and the score ranging from 0 to 4 was associated to each location. ICRS scores 0 and 1 were assigned to group 1 while ICRS scores 2 to 4 were assigned to group 2 (Table 3.1).

Table 3.1: Number of samples in each ICRS group

ICRS	Number of samples
0	0
1	14
2	10
3	3
4	0

As can be seen in the table 3.1, there were only few samples in ICRS score 3 group, and thus, ICRS 2 and 3 groups were pooled together. Based on the ICRS scoring, group 1 represents presumably healthy samples and group 2 represents presumably degenerated cartilage samples [66].

3.6.2 Equilibrium modulus based grouping

An additional grouping for the samples was conducted according to measured equilibrium modulus. PG loss is well-documented consequence of the OA progression and it is known that PG loss is the main cause of the decrease of the equilibrium modulus [45]. Based on this, the samples were grouped based on the equilibrium modulus which was obtained from literature review of healthy human cartilage tissue (Table 3.2). Based on the review and the location of the tissue samples (tibial cartilage), the samples were considered presumably as healthy (group 1) if $E_{eq} \geq 0.4$ MPa and osteoarthritic (group 2) if $E_{eq} < 0.4$ MPa.

Table 3.2: Literature review for human articular cartilage equilibrium modulus

Study	Reference	Sample location	Measurement geometry	Equilibrium modulus (MPa)	OA scoring system
Kleemann et al. 2005	[3]	Tibia	Unconfined compression	0.4-0.5	ICRS and Mankin
Stewart et al. 2017	[99]	Femur, Tibia and Patella	Indentation	0.54	Mankin and OARSI
Wilusz et al. 2013	[100]	Femur	Nano-indentation	0.1-0.3	Histological analysis
Wang et al. 2013	[101]	Femur	Nano-indentation	0.16	Outerbridge scoring system
Boschetti et al. 2008	[102]	Femur	Unconfined compression	0.42	Visual and touch inspection
Boschetti et al. 2004	[103]	Femur	Confined compression	0.25	Visual and touch inspection
Kiviranta et al. 2008	[9]	Patella	Indentation	0.64	Mankin
Armstrong et al. 1982	[4]	Patella	Confined compression	0.79	Mankin
Nissi et al. 2007	[104]	Patella	Unconfined compression	0.54	Visual inspection

3.6.3 Statistical Analysis

The normality of data was tested using Shapiro-Wilk test. As the grouped data (according to both ICRS-based and equilibrium modulus-based grouping) was not normally distributed, non-parametric tests were used. Friedman's two-way analysis of variance by ranks was used for testing differences in dynamic moduli at different frequencies. To compare the material parameters in different groups (ICRS score and E_{eq} based groupings), a pairwise comparison via Mann-Whitney U test was conducted. A two-tailed Pearson correlation analysis was used for testing correlations between material parameters. The level for statistical significance in all tests was set to $\alpha = 0.05$. Statistical analyses were performed using IBM SPSS Statistics (version 21, IBM Corporation, Armonk, NY, USA).

Chapter 4

Results

In this thesis, the human tibial cartilage was studied to evaluate the biomechanical behavior of cartilage. The first part of the study focused on the characterization of the compressive dynamic and equilibrium properties of the samples, and the second part aimed to quantify the contribution of the cartilage constituents on the biomechanical response of human cartilage using the FRPE material model through FE analysis and optimization. All data is presented as mean \pm standard deviation.

4.1 Elastic behavior of human tibial cartilage

Table 4.1: Elastic behavior of cartilage at equilibrium. Equilibrium modulus (E_{eq}) is presented as mean \pm standard deviation.

Classification		Number of samples	E_{eq} (MPa)
All samples		27	0.43 ± 0.44
ICRS-based	$ICRS \leq 1$	14	0.47 ± 0.52
	$ICRS > 1$	13	0.38 ± 0.33
Mechanical-based	$E_{eq} \geq 0.4$	10	0.86 ± 0.47
	$E_{eq} < 0.4$	17	0.17 ± 0.11

The mean value of equilibrium modulus calculated from all the samples was 0.43 ± 0.44 MPa ($n = 27$, Table 4.1). According to ICRS based classification of the samples, presumably healthy intact cartilage samples did not show significant different equilibrium modulus as compared to that of OA samples ($P > 0.05$). In mechanical-based grouping, presumably healthy intact cartilage samples showed significantly higher equilibrium modulus as compared to that of OA samples ($P < 0.001$).

4.2 Viscoelastic behavior of human tibial cartilage

Figure 4.1 represents the dynamic moduli of the human articular cartilage measured at different frequencies. The dynamic modulus of the samples at 0.005 Hz (0.97 ± 0.80 MPa) was significantly smaller ($P < 0.002$) compared to the dynamic moduli at frequencies 0.25, 0.625, 0.833 1 and 2 Hz. Similarly, the dynamic modulus of the samples at 0.05 Hz (1.20 ± 0.99 MPa) was significantly smaller ($P < 0.05$) than those of other frequencies except frequencies of 0.1 and 0.25 Hz. The dynamic moduli

of the samples at the frequencies of 0.1 and 0.25 Hz were significantly higher compared to those at 0.5, 0.625, 1 and 2 Hz ($P < 0.05$).

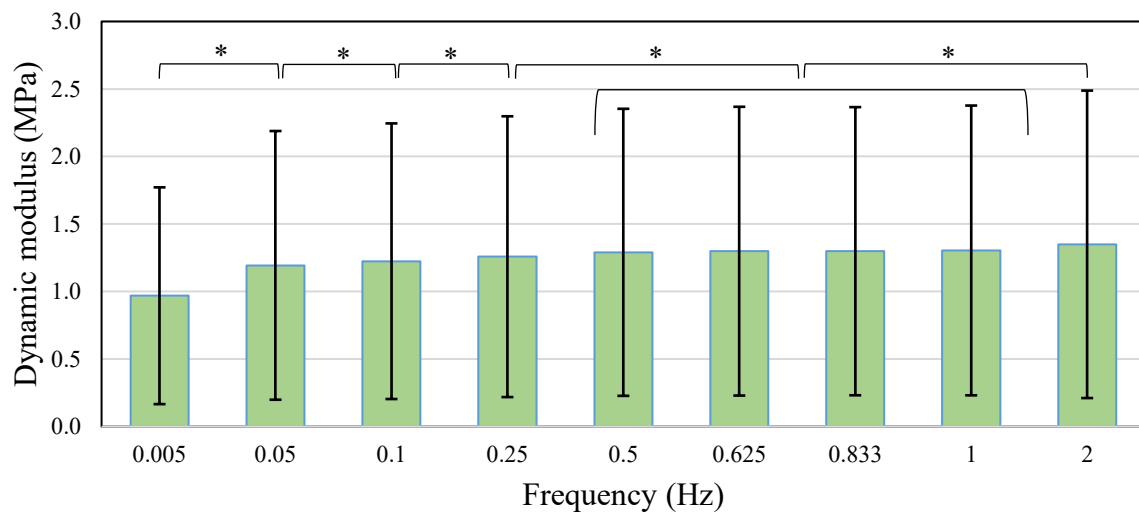


Figure 4.1: Dynamic modulus of human tibial cartilage as a function of loading frequency, * represents $P < 0.05$

The dynamic moduli of the samples at the frequencies equal or higher than 0.5 Hz were not different compared to each other, meaning that the dynamic modulus of human tibial cartilage reached a plateau at 1.3 MPa, approximately (Fig. 4.1, $P > 0.05$).

The phase difference between cyclic displacement and force response at 0.005 Hz was significantly higher than those at other frequencies ($P < 0.018$). The phase difference at the frequency of 0.05 Hz was significantly higher from those at frequencies of 0.833 and 1 Hz ($P < 0.008$).

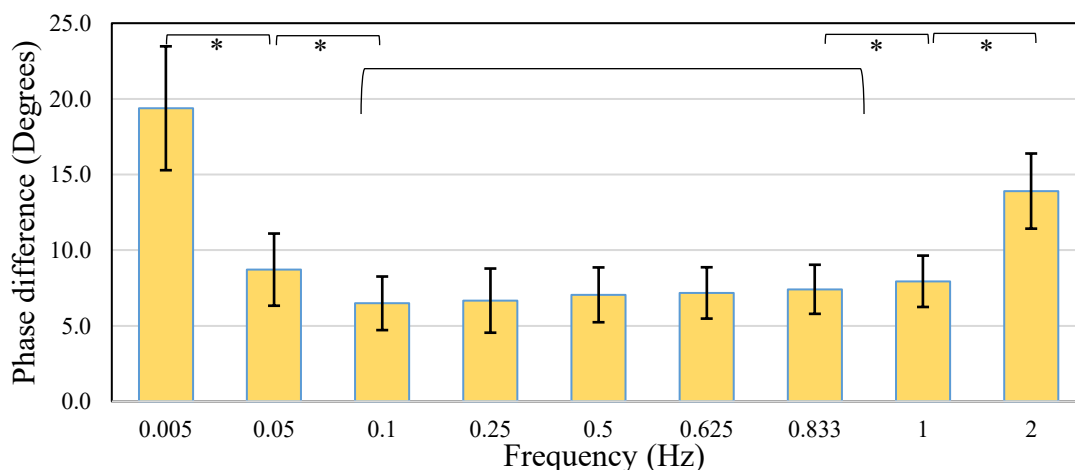


Figure 4.2: Phase difference of tibial cartilage in difference frequencies, * represents $P < 0.05$

The phase difference plateaued at the frequencies of 0.1 to 1 Hz, measuring 7 ± 0.48 degrees approximately ($P > 0.05$). The phase difference of 2 Hz frequency showed significantly higher value

compared to the phase difference at 1 Hz, measuring 13.9 and 7.9 degrees, respectively (Fig 4.2, $P < 0.05$).

4.2.1 ICRS-based grouping

The dynamic moduli of the samples, grouped according to ICRS scores are presented in Figure 4.3. There was no significant differences between the groups dynamic moduli at any frequency (Fig. 4.3, $P > 0.05$).

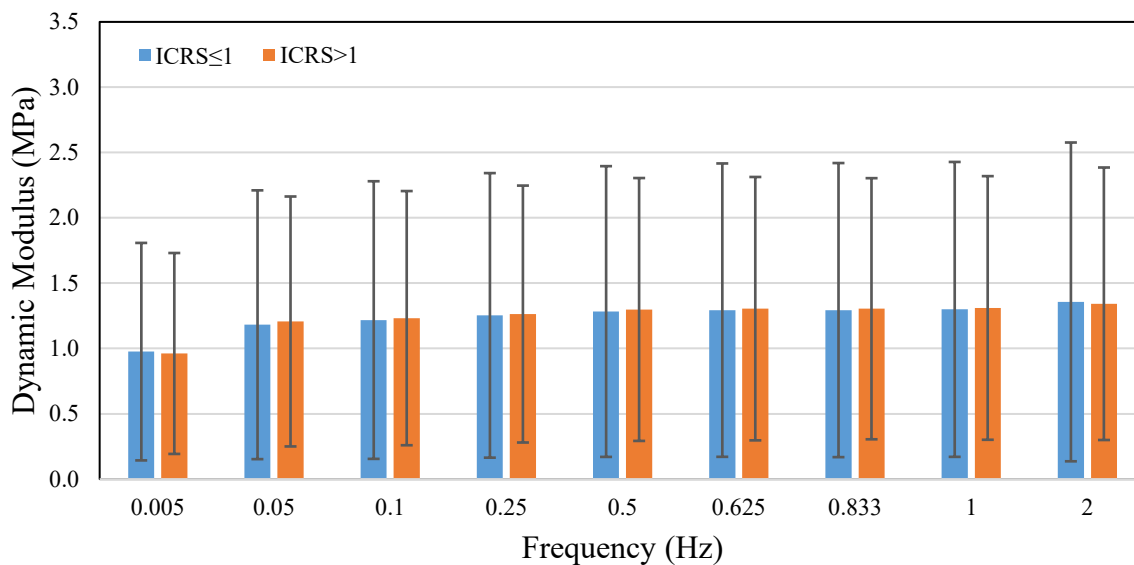


Figure 4.3: Dynamic moduli at different frequencies for different ICRS groups.

The phase differences between ICRS-based groups were not significantly different from each other except at 2 Hz (Figure 4.4). The presumably degenerated samples (ICRS > 1) showed higher phase difference (viscosity) at 2 Hz compared to presumably healthy (ICRS ≤ 1) cartilage samples ($P < 0.05$).

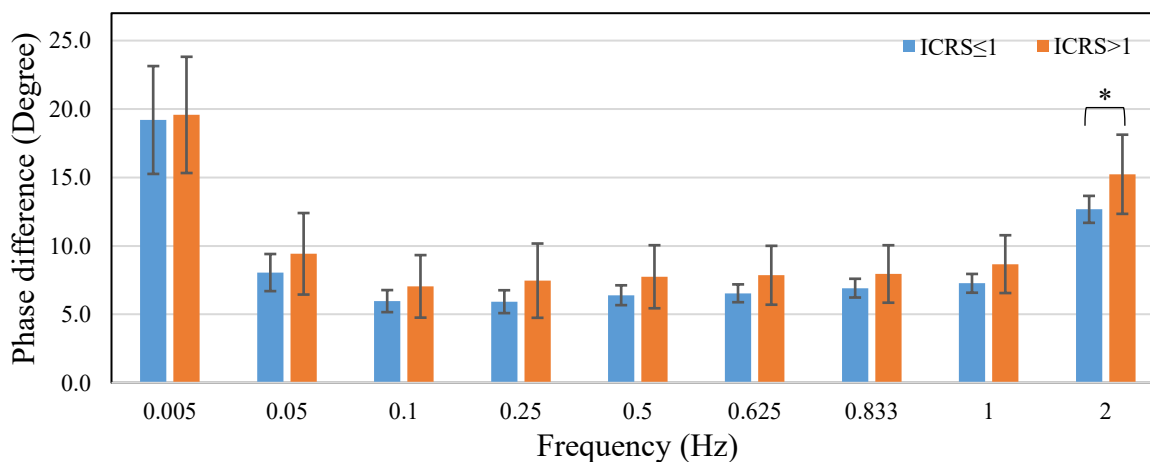


Figure 4.4: Phase difference between ICRS groups as a function of frequency, * represents $P < 0.05$

4.2.2 Equilibrium modulus based grouping

The dynamic moduli of human tibial samples were significantly different when categorized based on biomechanical properties (Fig. 4.5, $P < 0.001$). The dynamic modulus of presumably healthy tibial samples ($ICRS \leq 1$) was 3.56 times (256%) higher at 0.005 Hz compared to the presumably degenerated samples ($ICRS > 1$, $P < 0.05$). The dynamic moduli of presumably healthy samples were 3.40 and 3.46 times higher at 1 Hz ($P < 0.05$) and 2 Hz ($P < 0.05$), respectively, compared to the presumably degenerated samples. The rest of pair-wise comparisons showed quite similar results.

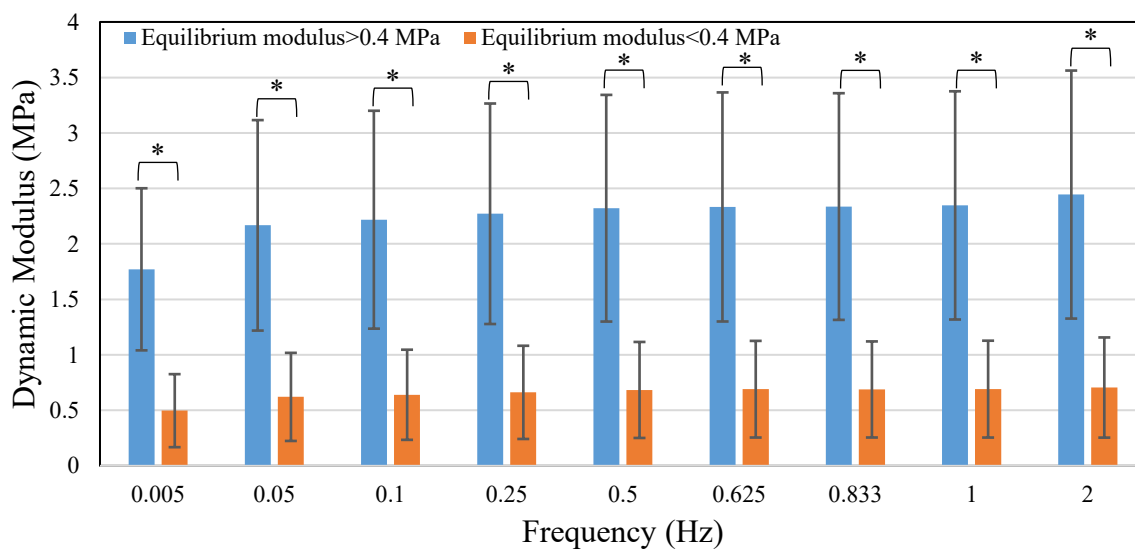


Figure 4.5: Dynamic modulus between equilibrium modulus groups as a function of frequency, * represents $P < 0.05$

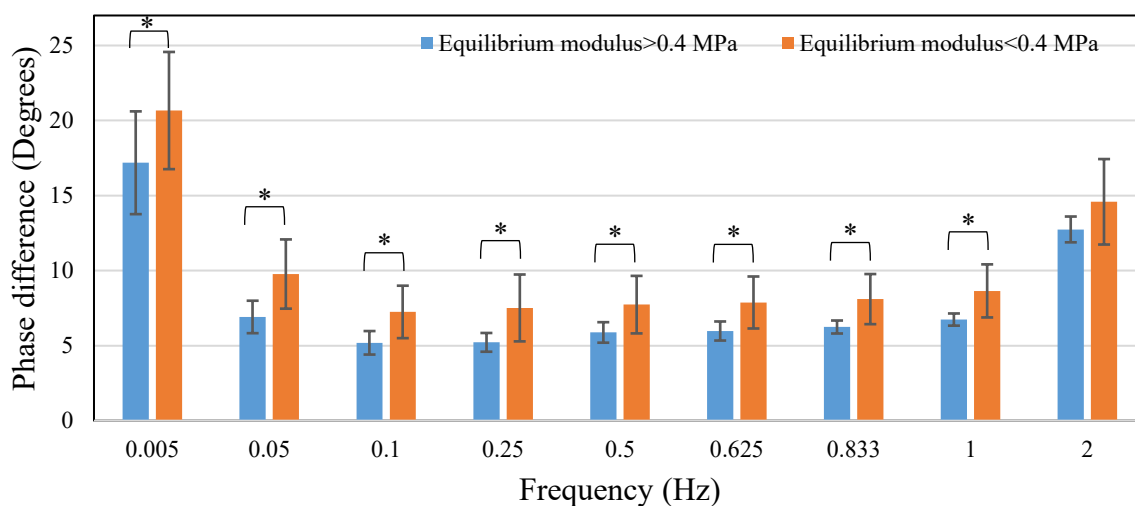


Figure 4.6: Phase difference between equilibrium modulus groups as a function of frequency, * represents $P < 0.05$

The presumably degenerated group ($E_{eq} < 0.4$ MPa) had significantly higher phase difference (viscosity) at all frequencies except at 2 Hz (*i.e.* from 0.005 Hz to 1 Hz) compared to the presumably

healthy group ($E_{eq} \geq 0.04$ MPa, $P < 0.05$, Fig. 4.6). The phase differences were approximately 20% to 41% higher in the presumably degenerated group compared to the presumably healthy group.

4.3 FRPE material properties

The optimized FRPE material parameters for all the samples ($n = 27$) are shown in Table 4.2, including the initial fibril network modulus (E_f^0) and its strain dependent modulus (E_f^ϵ), the non-fibrillar matrix modulus (E_{nf}), the initial permeability (k_0) and its strain-dependent factor (M).

Table 4.2: FRPE material parameters for human tibial cartilage ($n = 27$)

Material parameter	Related component	Mean \pm SD
E_f^0 (MPa)	Collagen	0.095 ± 0.222
E_f^ϵ (MPa)	Collagen	11.847 ± 10.356
E_{nf} (MPa)	Proteoglycan	0.117 ± 0.160
k_0 ($\times 10^{-15}$ m ⁴ /Ns)	Fluid	15.853 ± 19.867
M (-)	Fluid	3.663 ± 3.823

4.3.1 ICRS-based grouping

There were no statistically significant differences ($P > 0.05$) in the FRPE mechanical properties between the presumably healthy (ICRS ≤ 1) and degenerated (ICRS > 1) groups (Table 4.3).

Table 4.3: FRPE material parameters in the presumably healthy (ICRS ≤ 1) and degenerated (ICRS > 1) groups

Material parameter	Groups (ICRS)	Mean \pm SD	Statistical significance
E_f^0 (MPa)	≤ 1	0.12 ± 0.21	P=0.458
	> 1	0.07 ± 0.23	
E_f^ϵ (MPa)	≤ 1	9.38 ± 11.42	P=0.325
	> 1	13.48 ± 8.76	
E_{nf} (MPa)	≤ 1	0.12 ± 0.20	P=0.430
	> 1	0.11 ± 0.10	
k_0 (10^{-15} m ⁴ /N.s)	≤ 1	14.82 ± 14.59	P=0.685
	> 1	18.26 ± 24.09	
M (-)	≤ 1	2.89 ± 3.33	P=0.169
	> 1	4.72 ± 4.04	

E_f^0 : initial fibril network modulus, E_f^ϵ : strain-dependent fibril network modulus, E_{nf} : non-fibrillar matrix modulus, k_0 : initial permeability, M : permeability strain-dependent factor

4.3.2 Equilibrium modulus based grouping

In the equilibrium modulus based grouping, the initial fibril network modulus was not significantly different between the presumably healthy ($E_{eq} \geq 0.4$) and degenerated ($E_{eq} < 0.4$) groups ($P > 0.05$, Table 4.4). However, the strain-dependent fibril network modulus was 2.5 times higher in presumably healthy group compared to the presumably degenerated group ($P = 0.015$). The non-fibrillar matrix modulus was 5.8 times higher in the presumably healthy group compared to the degenerated one

($P < 0.001$). The initial permeability in the presumably degenerated group was 5.8 times higher compared to the presumably healthy group ($P = 0.001$), while there were no differences in the permeability strain-dependent factor between the groups ($P > 0.05$).

Table 4.4: FRPE material parameters in the presumably healthy ($E_{eq} \geq 0.4$) and degenerated ($E_{eq} < 0.4$) groups.

Material parameter	Groups	Mean \pm SD	Statistical significance
E_f^0 (MPa)	$E_{eq} \geq 0.4$	0.20 ± 0.31	$P > 0.05$
	$E_{eq} < 0.4$	0.03 ± 0.11	
E_f^ϵ (MPa)	$E_{eq} \geq 0.4$	19.09 ± 12.07	$P = 0.015$
	$E_{eq} < 0.4$	7.60 ± 5.95	
E_{nf} (MPa)	$E_{eq} \geq 0.4$	0.24 ± 0.21	$P < 0.001$
	$E_{eq} < 0.4$	0.04 ± 0.02	
k_0 (10^{-15} m ⁴ /N.s)	$E_{eq} \geq 0.4$	4.56 ± 4.85	$P = 0.001$
	$E_{eq} < 0.4$	22.65 ± 22.18	
M (-)	$E_{eq} \geq 0.4$	3.70 ± 2.85	$P > 0.05$
	$E_{eq} < 0.4$	3.64 ± 4.30	

E_f^0 : initial fibril network modulus, E_f^ϵ : strain-dependent fibril network modulus, E_{nf} : non-fibrillar matrix modulus, k_0 : initial permeability, M : permeability strain-dependent factor

Chapter 5

Discussion

The current study focused on quantification of the mechanical properties of human tibial cartilage. The samples were characterized **1)** by the elastic and viscoelastic biomechanical properties and **2)** by the fibril-reinforced poroelastic material properties, which can provide estimates about the roles of the tissue constituents on the mechanical behavior of the tissue. The bulk biomechanical properties of cartilage as well as the properties of its constituents were hypothesized to be correlated with the OA progression state as characterized either by visual inspection-based (ICRS scoring) or biomechanical-based (equilibrium modulus) methods.

The average equilibrium modulus of human tibial cartilage obtained in the current study is consistent with the literature where human tibial (0.4 MPa, [3]), femoral (0.42 MPa, [102]) or patellar (0.54 MPa, [104]) cartilage were studied. The equilibrium modulus of the tibial cartilage studied here is also well correlated with the non-fibrillar matrix modulus acquired from the modeling (Fig. 5.1), which is also consistent with earlier studies [83]. This can further validate the accuracy of model and material parameters optimization.

The dynamic modulus of the samples was the smallest at the lowest frequency (0.005 Hz), followed by a rapid increase in the dynamic modulus at 0.01 Hz. The dynamic modulus remained constant (1.3 ± 0.005 MPa) if the frequency was 0.5 Hz or higher. This confirms that the human cartilage dynamic modulus is unchanged within the physiological loading frequencies of daily routine activities (normal gait frequency: 1.1 Hz [105], fast gait frequency: 0.68 Hz [106]).

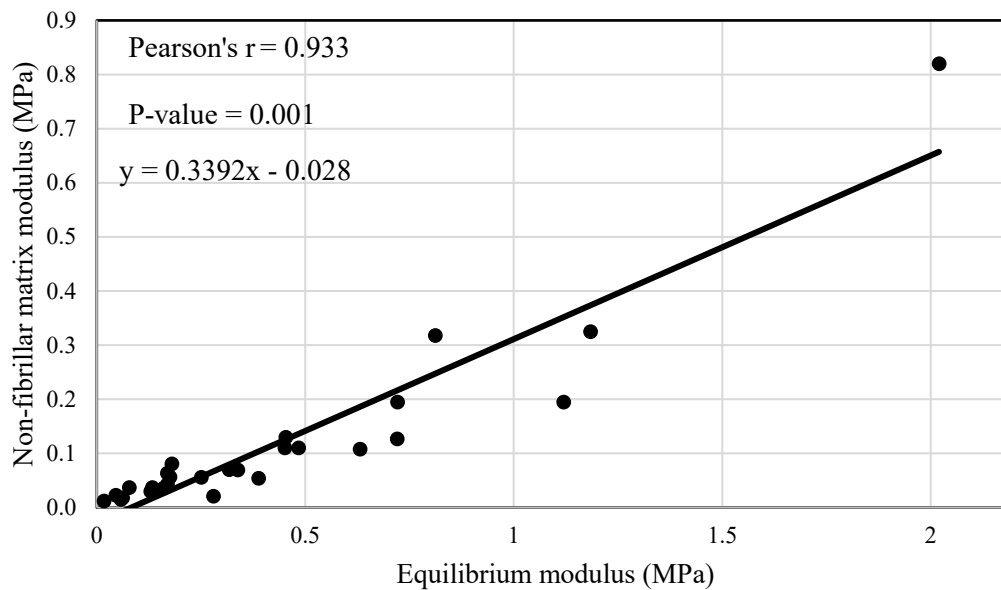


Figure 5.1: Pearson correlation between equilibrium and non-fibrillar matrix moduli.

The phase difference obtained from the dynamic test is a measure of the viscoelasticity of cartilage. The phase difference was highest (19.38 degrees) at the lowest frequency (0.005 Hz) followed by a phase difference plateau (7 ± 0.48 degrees) as the frequency increased. At the highest frequency (2 Hz) the phase difference started increasing once more (13.9 degrees). At a low frequency regime, the fluid is able to flow more freely and consequently, the cartilage exhibits a highly viscoelastic behavior with a high energy dissipation. As the frequency increases, the fluid flow is more restricted and the fluid pressurization and tension of collagen fibers are in charge of less viscous (*i.e.* more elastic) behavior. The phase difference plateau may be interpreted by the energy dissipation also in other constituents than interstitial fluid. Viscoelastic energy dissipation in the collagen fibers might be the reason for unaltered phase difference at higher frequencies as it has been reported for meniscus [107]. The constant phase difference at high frequencies has been also reported previously for other soft tissues, like meniscus [107,108]. To interpret the increase of the phase difference at the highest frequencies, one should consider the possible sources of error that might affect the results at this frequency. The cartilage may not be able to follow the indentation at unloading phase of cyclic loading that might lead to overestimation of the dynamic modulus.

The FRPE material properties obtained in the current study are comparable to previous literature values (*i.e.* initial network modulus and non-fibrillar matrix modulus) [45]. The permeability of the tibial cartilage ($15.9 \pm 19.9 \times 10^{-15} \frac{\text{m}^4}{\text{Ns}}$) was 4 times higher than that of reported for the hip joint cartilage ($3.6 \pm 2.9 \times 10^{-15} \frac{\text{m}^4}{\text{Ns}}$) [45]. That might be due to different OA stage or natural differences between human tibial and hip cartilage. In addition to that, the initial fibril network modulus, obtained in this study (0.1 ± 0.2 MPa) was lower compared to human hip joint cartilage [45]. That is likely to be a result of collagen

fibers fibrillation in the superficial zone of the cartilage, or it can be a result from natural differences between hip and tibial cartilage. The non-fibrillar matrix modulus was consistent with the studies conducted on human hip joint [45] and bovine articular cartilage [15,83,109].

Two different methods for sample groupings were used in this study. The first one was based on ICRS scoring based on visual inspection using arthroscopy, and the second one was based on the equilibrium modulus of cartilage known to reflect well the progression state of OA [45]. In the ICRS based grouping of the samples ($ICRS \leq 1$ and $ICRS > 1$), the equilibrium moduli of the samples were not significantly different between the groups. Moreover, the dynamic properties (dynamic modulus and the phase difference) were not significantly different except at the frequency of 2 Hz. In addition to the experimental biomechanical results, the FPRE properties of the samples obtained through FE modeling were not significantly different in between ICRS groups.

On the other hand, the equilibrium modulus based grouping of the samples showed good capability to distinguish between the presumably healthy and OA cartilage (*i.e.* $E_{eq} \geq 0.4$ MPa and $E_{eq} < 0.4$ MPa, respectively). The presumably OA group had significantly lower equilibrium modulus, which is indicating lower proteoglycan content within the tissue [7]. This result also is consistent with earlier studies [45,83]. The OA group also had significantly lower dynamic modulus and higher phase difference, which most likely indicates degeneration in the collagen network and/or changes in the fluid pressurization capability of cartilage [25]. High phase difference is associated with irreversible energy dissipation *i.e.* cartilage is not able to (reversibly) recover from the deformation [110]. The collagen network degradation and PG loss are shown to increase permeability [83], which could also lead to increase in the phase difference in cartilage.

The presumably healthy cartilage samples had significantly higher strain-dependent modulus than presumably OA samples according to the equilibrium modulus-based grouping, which is consistent with earlier studies in which they suggested that the strain-dependent fibril network modulus correlates with collagen content [83] and superficial collagen network orientation [45]. Besides, the non-fibrillar matrix modulus was significantly higher for the presumably healthy samples compared to the presumably osteoarthritic group, suggesting that the PG matrix was in a better condition in the health group. This is also consistent with the reported correlation of PG content and the non-fibrillar matrix modulus of cartilage in earlier studies [83]. Additionally, permeability in the presumably osteoarthritic group was significantly higher compared to the presumably healthy group. Recent studies have suggested that the permeability might be the first parameter susceptible to early OA changes [89]. Higher permeability has also been shown to be negatively correlated with the collagen content [45,83], which potentially supports the assumption that our equilibrium modulus-based grouping reflects better the state of OA degeneration.

The findings of the current study suggest that the ICRS-based grouping of the samples was not able to represent biomechanical changes in cartilage. In the arthroscopy and ICRS scoring, the appearance of tissue is evaluated (*i.e.* crack and fibrillation), which does not necessarily reflect alterations in osteoarthritic cartilage [62]. Furthermore, the cartilage samples were harvested from several locations of tibial plateau, both weight-bearing and non-weight-bearing locations of the tibial plateau. The ICRS scoring is based on the assessment of relatively large cartilage surface that does not necessarily reflect more localized site-specific properties of our cartilage samples with relatively smaller areas. The ICRS scoring is also dependent on the individual orthopedists' opinion and same cartilage may be scored differently by different orthopedists [111]. Histologic scoring methods, such as Mankin or OARSI scoring, could produce better results and obviously more specific information of local tissue structure and composition.

In conclusion, the results of this study provide novel quantitative knowledge of the mechanical properties of healthy and osteoarthritic human tibial cartilage. The cartilage material properties were shown to indicate the OA development when the samples were grouped based on their bulk equilibrium modulus. ICRS scoring based grouping did not indicate any significant differences in the tissue mechanical properties. Finally, novel FRPE mechanical parameters were characterized for human tibial cartilage, which can be used later for more accurate and detailed modeling of the mechanical behavior of cartilage *e.g.* in computational models of the knee joint. In the future, we will establish structure-function relationships in human tibial cartilage using microscopic and spectroscopic methods.

Appendix A.

Table A.1: Dynamic test results for samples 1-14, dynamic moduli ($D[f]$) and phase difference ($P[f]$) as a function of frequency f , E group: equilibrium modulus based grouping.

Sample ID	Patient	E group	ICRS	D(0.005)	P(0.005)	D(0.05)	P(0.05)	D(0.1)	P(0.1)	D(0.25)	P(0.25)	D(0.5)	P(0.5)	D(0.625)	P(0.625)	D(0.833)	P(0.833)	D(1)	P(1)	D(2)	P(2)
1	1	1	1	1.659	17.391	1.858	6.562	1.891	4.985	1.953	5.421	1.985	6.355	1.987	5.676	1.993	6.362	2.008	6.539	2.122	12.901
2	1	2	1	0.458	18.389	0.524	7.667	0.543	5.688	0.561	5.353	0.578	5.884	0.583	6.414	0.580	6.177	0.585	6.473	0.562	12.971
3	1	1	1	0.878	13.356	0.987	5.690	1.022	4.600	1.036	4.783	1.056	5.615	1.065	5.980	1.070	6.262	1.070	6.716	1.108	13.544
4	1	2	1	0.773	27.092	0.975	10.365	1.024	7.289	1.054	7.171	1.085	7.584	1.105	7.447	1.100	7.583	1.099	8.040	1.090	12.860
5	1	2	1	0.351	21.995	0.440	9.570	0.450	6.512	0.466	7.008	0.478	7.260	0.483	6.789	0.481	7.515	0.482	7.959	0.503	12.445
6	2	1	1	1.282	13.470	1.542	6.704	1.561	5.679	1.625	6.149	1.662	6.912	1.664	6.323	1.681	7.019	1.696	7.374	1.758	12.351
7	2	2	1	0.639	18.856	0.737	8.193	0.756	6.148	0.776	6.711	0.795	7.010	0.799	6.979	0.795	7.668	0.798	8.175	0.829	15.144
8	3	1	1	3.123	15.038	3.872	6.908	4.023	5.497	4.087	4.995	4.195	6.108	4.228	6.653	4.216	6.865	4.247	6.918	4.599	11.457
9	4	2	1	0.135	19.801	0.180	10.236	0.185	7.845	0.198	7.332	0.204	7.208	0.205	7.878	0.204	8.278	0.205	8.430	0.202	13.344
10	4	1	1	2.1370	24.583	2.742	8.888	2.814	6.232	2.940	5.906	2.979	5.940	3.028	5.401	3.061	5.662	3.031	6.336	3.197	11.406
11	5	2	1	0.667	21.530	0.884	8.710	0.919	5.896	0.934	6.064	0.969	6.260	0.973	6.750	0.962	6.985	0.978	7.140	1.020	11.961
12	6	2	1	1.303	21.801	1.489	7.602	1.529	5.618	1.581	4.912	1.627	4.808	1.637	7.014	1.621	6.805	1.6433	6.487	1.679	11.656
13	5	2	1	0.132	20.281	0.167	8.441	0.176	5.717	0.177	6.007	0.182	6.591	0.187	6.183	0.184	6.344	0.183	7.389	0.164	11.862
14	5	2	1	0.116	15.182	0.141	7.203	0.146	5.836	0.151	5.139	0.156	6.012	0.157	6.039	0.158	7.266	0.158	7.750	0.153	13.479

Table A.2: Dynamic test results for samples 15-27, dynamic moduli ($D(f)$) and phase difference ($P(f)$) as a function of frequency f , E group: equilibrium modulus based grouping.

Sample ID	E group	D(0.005)	D(0.05)	D(0.1)	D(0.25)	D(0.5)	D(0.625)	D(0.833)	D(1)	D(2)
Patient	ICRS	P(0.005)	P(0.05)	P(0.1)	P(0.25)	P(0.5)	P(0.625)	P(0.833)	P(1)	P(2)
15	1	1.158	1.247	1.283	1.308	1.331	1.337	1.350	1.343	1.384
1	2	14.479	5.925	4.610	5.097	5.730	6.638	6.147	6.974	14.227
16	2	0.898	1.053	1.062	1.103	1.128	1.137	1.124	1.134	1.211
2	2	18.175	7.385	5.559	6.184	6.859	7.152	6.697	7.699	14.571
17	2	0.772	1.057	1.074	1.115	1.144	1.144	1.149	1.143	1.198
2	2	20.060	9.018	6.371	6.356	7.292	6.965	7.988	8.496	14.521
18	2	0.172	0.235	0.247	0.256	0.268	0.274	0.272	0.271	0.280
3	2	20.490	13.509	9.915	10.443	10.485	10.074	10.911	10.945	20.115
19	2	0.029	0.040	0.046	0.046	0.046	0.048	0.049	0.048	0.049
3	2	13.065	11.180	10.135	11.380	10.805	11.115	8.445	11.669	13.755
20	2	0.286	0.325	0.332	0.344	0.354	0.356	0.355	0.355	0.366
5	2	16.837	7.287	6.115	5.933	6.460	6.891	7.017	7.579	14.378
21	2	0.657	0.903	0.916	0.950	0.986	1.003	1.006	0.999	0.963
6	2	28.270	13.294	10.047	10.081	9.532	9.244	10.680	10.669	17.041
22	1	1.533	2.131	2.176	2.227	2.294	2.305	2.298	2.318	2.411
7	2	21.556	8.522	6.301	5.789	6.371	6.579	6.368	7.028	13.122
23	2	0.515	0.688	0.734	0.753	0.800	0.817	0.826	0.828	0.877
6	2	23.257	14.651	10.324	12.282	11.812	12.118	12.273	12.761	22.581
24	2	0.546	0.719	0.742	0.785	0.821	0.829	0.832	0.840	0.847
6	2	26.237	11.808	8.198	9.374	9.597	8.841	9.085	9.367	15.280
25	1	1.026	1.335	1.360	1.411	1.428	1.425	1.444	1.449	1.487
7	2	18.033	7.481	5.558	5.269	5.737	5.648	5.970	7.122	13.029
26	1	2.011	2.263	2.267	2.303	2.362	2.346	2.348	2.375	2.249
7	2	15.934	5.413	3.616	3.851	4.162	4.552	5.589	5.940	12.117
27	1	2.902	3.693	3.781	3.824	3.920	3.942	3.902	3.931	4.128
7	2	18.030	7.030	4.817	4.940	5.871	6.302	6.171	6.435	13.293

Appendix B.

Table B.1: FRPE material properties for samples 1-14, E_P^0 : initial fibril network modulus, E_P^f : strain-dependent fibril network modulus, E_{nf} : non-fibrillar matrix modulus, k_0 : initial permeability, M : permeability strain-dependent factor, M: Medial, L: Lateral, A: Anterior, C: Central, P: Posterior and D: Distal.

Sample ID	Patient ID	Cartilage site	Cartilage thickness	ICRS score	Mechanical -based group	E_P^0 (MPa)	E_P^f (MPa)	E_{nf} (MPa)	$k_0 \times 10^{-15}$ (m ² /N.s)	M (-)
1	1	LA*	3.203	1	1	0.152	22.7	0.108	0.63	0.0033
2	1	LC*	3.475	1	2	0.000001	8.24000	0.03600	3.80	0.81000
3	1	MC*	3.750	1	1	0.000001	10.41	0.11	16.7	9.8
4	1	LA	3.641	1	2	0.043	19.34	0.07	1.7	0.3
5	1	MC	2.812	1	2	0.000002	5.4	0.03	46	0.0005
6	2	LA	2.812	1	1	0.32	0.087	0.195	1.3	7.16
7	2	LC	4.265	1	2	0.031	6.9	0.021	15	3.93
8	3	LC	2.422	1	1	0.69	5.14	0.82	1.2	2.83
9	4	LC	3.000	1	2	0.000002	1.28	0.015	13	0.12
10	4	MC	2.406	1	1	0.000001	44.36	0.127	4.5	0.254
11	5	MC	2.531	1	2	0.00008	11.71	0.056	16	8.17
12	6	LC	2.703	1	2	0.468	6.463	0.0697	6.4	4.1796
13	5	LC	3.390	1	2	0.00002	1.4848	0.02288	45.2	0.0011
14	5	LC	4.375	1	2	0.000001	1.1259	0.018	21.9	0.00000001

Table B.2: FRPE material properties for samples 15-27, E_f^0 : initial fibril network modulus, E_f^ϵ : strain-dependent fibril network modulus, E_{nf} : non-fibrillar matrix modulus, k_0 : initial permeability, M : permeability strain-dependent factor, M: Medial, L: Lateral, A: Anterior, C: Central, P: Posterior and D: Distal.

Sample ID	Patient ID	Cartilage site	Cartilage thickness	ICRS score	Mechanical -based group	E_f^0 (MPa)	E_f^ϵ (MPa)	E_{nf} (MPa)	$k_0 \times 10^{-15}$ (m ⁴ /N.s)	M (-)
15	1	LC	4.812	2	1	0.000003	18.07	0.11	3.5	3.62
16	2	LC	3.625	2	2	0.000004	16.27	0.054	17	2.09
17	2	MC	2.565	2	2	0.000001	11.46	0.081	10.7	3.47
18	3	MC	1.797	2	2	0.000083	1.1	0.037	4.9	0.0017
19	3	LC	2.109	2	2	0.0033	0.074	0.012	10.6	0.0008
20	5	MC	3.516	2	2	0.000002	4.04	0.037	16.7	5.27
21	6	MC	2.422	2	2	0.000004	18.13	0.0428	78.1	14.061
22	7	MC	2.547	2	1	0.00009	26.05	0.195	10	4.22
23	6	MP*	1.766	2	2	0.000007	6.259	0.0638	9.3	8.022
24	6	LC	2.375	2	2	0.000122	9.741	0.0564	68.8	11.517
25	7	MC	2.531	3	1	0.000008	14.86	0.13	5	2.3
26	7	LD*	3.140	3	1	0.000001	29.4364	0.318	1.49	4.65977
27	7	LD	2.578	3	1	0.873	19.758	0.325	1.321	2.122

Bibliography

- [1] A.P. Newman, Articular cartilage repair, *Am. J. Sports Med.* 26 (1998) 309–324.
- [2] K.A. Esmonde-White, G.S. Mandair, F. Raaij, J.A. Jacobson, B.S. Miller, A.G. Urquhart, B.J. Roessler, M.D. Morris, Raman spectroscopy of synovial fluid as a tool for diagnosing osteoarthritis, *J. Biomed. Opt.* 14 (2009) 34013.
- [3] R.U. Kleemann, D. Krocker, A. Cedraro, J. Tuischer, G.N. Duda, Altered cartilage mechanics and histology in knee osteoarthritis: relation to clinical assessment (ICRS Grade), *Osteoarthr. Cartil.* 13 (2005) 958–963.
- [4] C.G. Armstrong, V.C. Mow, Variations in the intrinsic mechanical properties of human articular cartilage with age, degeneration, and water content., *J. Bone Joint Surg. Am.* 64 (1982) 88–94. <http://www.ncbi.nlm.nih.gov/pubmed/7054208>.
- [5] J. Desrochers, M.A. Amrein, J.R. Matyas, Structural and functional changes of the articular surface in a post-traumatic model of early osteoarthritis measured by atomic force microscopy, *J. Biomech.* 43 (2010) 3091–3098.
- [6] M. Stolz, R. Gottardi, R. Raiteri, S. Miot, I. Martin, R. Imer, U. Staufer, A. Raducanu, M. Düggelein, W. Baschong, Early detection of aging cartilage and osteoarthritis in mice and patient samples using atomic force microscopy, *Nat. Nanotechnol.* 4 (2009) 186.
- [7] P. Julkunen, W. Wilson, J.S. Jurvelin, J. Rieppo, C.-J. Qu, M.J. Lammi, R.K. Korhonen, Stress–relaxation of human patellar articular cartilage in unconfined compression: prediction of mechanical response by tissue composition and structure, *J. Biomech.* 41 (2008) 1978–1986.
- [8] V.C. Mow, S.C. Kuei, W.M. Lai, C.G. Armstrong, Biphasic creep and stress relaxation of articular cartilage in compression: theory and experiments, *J Biomech Eng.* 102 (1980) 73–84.
- [9] P. Kiviranta, E. Lammentausta, J. Töyräs, I. Kiviranta, J.S. Jurvelin, Indentation diagnostics of cartilage degeneration, *Osteoarthr. Cartil.* 16 (2008) 796–804. doi:10.1016/j.joca.2007.10.016.
- [10] P. Kiviranta, J. Rieppo, R.K. Korhonen, P. Julkunen, J. Töyräs, J.S. Jurvelin, Collagen network primarily controls Poisson’s ratio of bovine articular cartilage in compression, *J. Orthop. Res.* 24 (2006) 690–699.
- [11] V.C. Mow, A. Ratcliffe, A.R. Poole, Cartilage and diarthrodial joints as paradigms for

- hierarchical materials and structures, *Biomaterials*. 13 (1992) 67–97.
- [12] M.A. Soltz, G.A. Ateshian, Interstitial fluid pressurization during confined compression cyclical loading of articular cartilage, *Ann. Biomed. Eng.* 28 (2000) 150–159.
- [13] J.A. Buckwalter, Osteoarthritis and articular cartilage use, disuse, and abuse: experimental studies., *J. Rheumatol. Suppl.* 43 (1995) 13–15.
- [14] S. Saarakkala, P. Julkunen, P. Kiviranta, J. Mäkitalo, J.S. Jurvelin, R.K. Korhonen, Depth-wise progression of osteoarthritis in human articular cartilage: investigation of composition, structure and biomechanics, *Osteoarthr. Cartil.* 18 (2010) 73–81.
- [15] R.K. Korhonen, M.S. Laasanen, J. Töyräs, R. Lappalainen, H.J. Helminen, J.S. Jurvelin, Fibril reinforced poroelastic model predicts specifically mechanical behavior of normal, proteoglycan depleted and collagen degraded articular cartilage, *J. Biomech.* 36 (2003) 1373–1379.
- [16] W. Wilson, C.C. Van Donkelaar, B. Van Rietbergen, K. Ito, R. Huiskes, Stresses in the local collagen network of articular cartilage: a poroviscoelastic fibril-reinforced finite element study, *J. Biomech.* 37 (2004) 357–366.
- [17] P. Julkunen, T. Harjula, J. Marjanen, H.J. Helminen, J.S. Jurvelin, Comparison of single-phase isotropic elastic and fibril-reinforced poroelastic models for indentation of rabbit articular cartilage, *J. Biomech.* 42 (2009) 652–656.
- [18] K.S. Saladin, L. Miller, *Anatomy & physiology*, WCB/McGraw-Hill New York (NY), 1998.
- [19] P.J. Rasch, M.D. Grabiner, R.J. Gregor, J. Garhammer, *Kinesiology and applied anatomy*, Lea & Febiger, 1989.
- [20] R.J. Last, Some anatomical details of the knee joint., *J. Bone Jt. Surg.* 30B (1948) 683–688.
- [21] R.S. Behnke, *Kinetic Anatomy 3rd Edition*, Human Kinetics, 2012.
- [22] M.D. Jeffrey H. Berg, *Patellar Instability - Anatomy and Causes* - Jeffrey H. Berg, M.D., (2014). <https://www.jeffreybergmd.com/patellar-instability/> (accessed February 5, 2018).
- [23] D.L. Butler, F.R. Noyes, E.S. Grood, Ligamentous restraints to anterior-posterior drawer in the human knee. A biomechanical study., *JBJS.* 62 (1980) 259–270.
- [24] A.J. Sophia Fox, A. Bedi, S.A. Rodeo, *The basic science of articular cartilage: structure,*

- composition, and function, *Sports Health*. 1 (2009) 461–468.
- [25] A.D. Pearle, R.F. Warren, S.A. Rodeo, Basic science of articular cartilage and osteoarthritis, *Clin. Sports Med.* 24 (2005) 1–12.
- [26] J.A. Buckwalter, H.J. Mankin, Articular cartilage: tissue design and chondrocyte-matrix interactions., *Instr. Course Lect.* 47 (1998) 477–486.
- [27] J.P.G. Urban, The chondrocyte: a cell under pressure, *Rheumatology*. 33 (1994) 901–908.
- [28] H. Muir, The chondrocyte, architect of cartilage. Biomechanics, structure, function and molecular biology of cartilage matrix macromolecules, *Bioessays*. 17 (1995) 1039–1048.
- [29] V.C. Mow, R. Huiskes, *Basic orthopaedic biomechanics & mechano-biology*, Lippincott Williams & Wilkins, 2005.
- [30] V.C. Mow, M.H. Holmes, W.M. Lai, Fluid transport and mechanical properties of articular cartilage: a review, *J. Biomech.* 17 (1984) 377–394.
- [31] C. Glaser, R. Putz, Functional anatomy of articular cartilage under compressive loading Quantitative aspects of global, local and zonal reactions of the collagenous network with respect to the surface integrity, *Osteoarthr. Cartil.* 10 (2002) 83–99.
- [32] D.R. Eyre, The collagens of articular cartilage, in: *Semin. Arthritis Rheum.*, Elsevier, 1991: pp. 2–11.
- [33] B.M. Nigg, W. Herzog, *Biomechanics of the musculo-skeletal system*, John Wiley & Sons, 2007.
- [34] J.A. Buckwalter, H.J. Mankin, Articular Cartilage: Part I Tissue Design and Chondrocyte-Matrix Interactions, *JBJS*. 79 (1997) 600–611.
- [35] M.J. Kääh, I. Ap Gwynn, H.P. Nötzli, Collagen fibre arrangement in the tibial plateau articular cartilage of man and other mammalian species, *J. Anat.* 193 (1998) 23–34.
- [36] R. Shirazi, A. Shirazi-Adl, M. Hurtig, Role of cartilage collagen fibrils networks in knee joint biomechanics under compression, *J. Biomech.* 41 (2008) 3340–3348.
- [37] K.A. Athanasiou, M.P. Rosenwasser, J.A. Buckwalter, T.I. Malinin, V.C. Mow, Interspecies comparisons of in situ intrinsic mechanical properties of distal femoral cartilage, *J. Orthop. Res.* 9 (1991) 330–340.

- [38] L.P. Räsänen, M.E. Mononen, M.T. Nieminen, E. Lammentausta, J.S. Jurvelin, R.K. Korhonen, Implementation of subject-specific collagen architecture of cartilage into a 2D computational model of a knee joint—data from the osteoarthritis initiative (OAI), *J. Orthop. Res.* 31 (2013) 10–22.
- [39] M.S. Venäläinen, Computational modeling of knee joint function based on CT arthrography, 2017.
- [40] W. Wilson, C.C. Van Donkelaar, B. Van Rietbergen, R. Huiskes, A fibril-reinforced poroviscoelastic swelling model for articular cartilage, *J. Biomech.* 38 (2005) 1195–1204.
- [41] R.J. Wilkins, J.A. Browning, J.P.G. Urban, Chondrocyte regulation by mechanical load, *Biorheology.* 37 (2000) 67–74.
- [42] P. Tanska, Cell-tissue interactions and adaptation in cartilage, 2016.
- [43] M.A. Soltz, G.A. Ateshian, Experimental verification and theoretical prediction of cartilage interstitial fluid pressurization at an impermeable contact interface in confined compression, *J. Biomech.* 31 (1998) 927–934.
- [44] S. Park, R. Krishnan, S.B. Nicoll, G.A. Ateshian, Cartilage interstitial fluid load support in unconfined compression, *J. Biomech.* 36 (2003) 1785–1796.
- [45] J.T.A. Mäkelä, M.R.J. Huttu, R.K. Korhonen, Structure–function relationships in osteoarthritic human hip joint articular cartilage, *Osteoarthr. Cartil.* 20 (2012) 1268–1277.
- [46] J.M. Mansour, Biomechanics of cartilage, *Kinesiol. Mech. Pathomechanics Hum. Mov.* (2003) 66–79.
- [47] W.C. Hayes, A.J. Bodine, Flow-independent viscoelastic properties of articular cartilage matrix, *J. Biomech.* 11 (1978) 407–419.
- [48] S. Park, C.T. Hung, G.A. Ateshian, Mechanical response of bovine articular cartilage under dynamic unconfined compression loading at physiological stress levels, *Osteoarthr. Cartil.* 12 (2004) 65–73.
- [49] E.M. Hasler, W. Herzog, J.Z. Wu, W. Müller, U. Wyss, Articular cartilage biomechanics: theoretical models, material properties, and biosynthetic response., *Crit. Rev. Biomed. Eng.* 27 (1999) 415–488.
- [50] S.-Y. Woo, W.H. Akeson, G.F. Jemmott, Measurements of nonhomogeneous, directional

- mechanical properties of articular cartilage in tension, *J. Biomech.* 9 (1976) 785–791.
- [51] J.C. Mansfield, J.S. Bell, C.P. Winlove, The micromechanics of the superficial zone of articular cartilage, *Osteoarthr. Cartil.* 23 (2015) 1806–1816.
- [52] Y. Zhang, J.M. Jordan, Epidemiology of osteoarthritis, *Clin. Geriatr. Med.* 26 (2010) 355–369.
- [53] G. Balint, B. Szebenyi, Diagnosis of osteoarthritis, *Drugs.* 52 (1996) 1–13.
- [54] F.J. Blanco, R. Guitian, E. Vázquez-Martul, F.J. de Toro, F. Galdo, Osteoarthritis chondrocytes die by apoptosis: a possible pathway for osteoarthritis pathology, *Arthritis Rheumatol.* 41 (1998) 284–289.
- [55] N.A. Sharkey, N.I. Williams, J.B. Guerin, The role of exercise in the prevention and treatment of osteoporosis and osteoarthritis., *Nurs. Clin. North Am.* 35 (2000) 209–221.
- [56] M.C. Hochberg, R.D. Altman, K.D. Brandt, B.M. Clark, P.A. Dieppe, M.R. Griffin, R.W. Moskowitz, T.J. Schnitzer, Guidelines for the medical management of osteoarthritis, *Arthritis Rheumatol.* 38 (1995) 1535–1540.
- [57] P. Sarzi-Puttini, M.A. Cimmino, R. Scarpa, R. Caporali, F. Parazzini, A. Zaninelli, F. Atzeni, B. Canesi, Osteoarthritis: an overview of the disease and its treatment strategies, in: *Semin. Arthritis Rheum.*, Elsevier, 2005: pp. 1–10.
- [58] J. Clouet, C. Vinatier, C. Merceron, M. Pot-vaucel, Y. Maugars, P. Weiss, G. Grimandi, J. Guicheux, From osteoarthritis treatments to future regenerative therapies for cartilage, *Drug Discov. Today.* 14 (2009) 913–925.
- [59] D.B. Burr, E.L. Radin, Microfractures and microcracks in subchondral bone: are they relevant to osteoarthrosis?, *Rheum. Dis. Clin.* 29 (2003) 675–685.
- [60] R. Stoop, P. Buma, P.M. Van Der Kraan, A.P. Hollander, R.C. Billingham, T.H.M. Meijers, A.R. Poole, W.B. Van Den Berg, Type II collagen degradation in articular cartilage fibrillation after anterior cruciate ligament transection in rats, *Osteoarthr. Cartil.* 9 (2001) 308–315.
- [61] F. Guilak, A. Ratcliffe, N. Lane, M.P. Rosenwasser, V.C. Mow, Mechanical and biochemical changes in the superficial zone of articular cartilage in canine experimental osteoarthritis, *J. Orthop. Res.* 12 (1994) 474–484.
- [62] E. Calvo, I. Palacios, E. Delgado, J. Ruiz-Cabello, P. Hernandez, O. Sanchez-Pernaute, J. Egido, G. Herrero-Beaumont, High-resolution MRI detects cartilage swelling at the early

- stages of experimental osteoarthritis, *Osteoarthr. Cartil.* 9 (2001) 463–472.
- [63] J.A. Buckwalter, H.J. Mankin, Articular cartilage: degeneration and osteoarthritis, repair, regeneration, and transplantation., *Instr. Course Lect.* 47 (1998) 487–504.
- [64] J.C. de Grauw, C.H.A. van de Lest, P.R. van Weeren, Inflammatory mediators and cartilage biomarkers in synovial fluid after a single inflammatory insult: a longitudinal experimental study, *Arthritis Res. Ther.* 11 (2009) R35.
- [65] R. Altman, E. Asch, D. Bloch, G. Bole, D. Borenstein, K. Brandt, W. Christy, T.D. Cooke, R. Greenwald, M. Hochberg, Development of criteria for the classification and reporting of osteoarthritis: classification of osteoarthritis of the knee, *Arthritis Rheumatol.* 29 (1986) 1039–1049.
- [66] M. Brittberg, C.S. Winalski, Evaluation of cartilage injuries and repair, *JBJS.* 85 (2003) 58–69.
- [67] P. Mainil-Varlet, T. Aigner, M. Brittberg, P. Bullough, A. Hollander, E. Hunziker, R. Kandel, S. Nehrer, K. Pritzker, S. Roberts, Histological assessment of cartilage repair: a report by the Histology Endpoint Committee of the International Cartilage Repair Society (ICRS), *JBJS.* 85 (2003) 45–57.
- [68] S.L.-Y. Woo, J.M. Hollis, D.J. Adams, R.M. Lyon, S. Takai, Tensile properties of the human femur-anterior cruciate ligament-tibia complex: The effects of specimen age and orientation, *Am. J. Sports Med.* 19 (1991) 217–225. doi:10.1177/036354659101900303.
- [69] R.K. Korhonen, M.S. Laasanen, J. Töyräs, J. Rieppo, J. Hirvonen, H.J. Helminen, J.S. Jurvelin, Comparison of the equilibrium response of articular cartilage in unconfined compression, confined compression and indentation, *J. Biomech.* 35 (2002) 903–909.
- [70] X.L. Lu, V.C. Mow, Biomechanics of articular cartilage and determination of material properties, *Med. Sci. Sport. Exerc.* 40 (2008) 193–199.
- [71] M.R. DiSilvestro, J.-K.F. Suh, A cross-validation of the biphasic poroviscoelastic model of articular cartilage in unconfined compression, indentation, and confined compression, *J. Biomech.* 34 (2001) 519–525.
- [72] R.K. Korhonen, S. Saarakkala, Biomechanics and modeling of skeletal soft tissues, in: *Theor. Biomech.*, InTech, 2011.
- [73] N.P. Cohen, R.J. Foster, V.C. Mow, Composition and dynamics of articular cartilage:

- structure, function, and maintaining healthy state, *J. Orthop. Sport. Phys. Ther.* 28 (1998) 203–215.
- [74] W.C. Hayes, L.M. Keer, G. Herrmann, L.F. Mockros, A mathematical analysis for indentation tests of articular cartilage, *J. Biomech.* 5 (1972) 541–551.
- [75] K.K. Chawla, M.A. Meyers, *Mechanical behavior of materials*, Prentice Hall, 1999.
- [76] P.M. Bursać, T.W. Obitz, S.R. Eisenberg, D. Stamenović, Confined and unconfined stress relaxation of cartilage: appropriateness of a transversely isotropic analysis, *J. Biomech.* 32 (1999) 1125–1130.
- [77] B. Cohen, W.M. Lai, V.C. Mow, A transversely isotropic biphasic model for unconfined compression of growth plate and chondroepiphysis, *J. Biomech. Eng.* 120 (1998) 491–496.
- [78] L.P. Li, M.D. Buschmann, A. Shirazi-Adl, A fibril reinforced nonhomogeneous poroelastic model for articular cartilage: inhomogeneous response in unconfined compression, *J. Biomech.* 33 (2000) 1533–1541.
- [79] E.K. Danso, J.T.J. Honkanen, S. Saarakkala, R.K. Korhonen, Comparison of nonlinear mechanical properties of bovine articular cartilage and meniscus, *J. Biomech.* 47 (2014) 200–206. doi:10.1016/j.jbiomech.2013.09.015.
- [80] X. Chen, Y. Zhou, L. Wang, M.H. Santare, L.Q. Wan, X.L. Lu, Determining tension–compression nonlinear mechanical properties of articular cartilage from indentation testing, *Ann. Biomed. Eng.* 44 (2016) 1148–1158.
- [81] M.H. Holmes, V.C. Mow, The nonlinear characteristics of soft gels and hydrated connective tissues in ultrafiltration, *J. Biomech.* 23 (1990) 1145–1156.
- [82] A. Grillo, M. Carfagna, S. Federico, Non-Darcian flow in fibre-reinforced biological tissues, *Meccanica.* 52 (2017) 3299–3320.
- [83] P. Julkunen, P. Kiviranta, W. Wilson, J.S. Jurvelin, R.K. Korhonen, Characterization of articular cartilage by combining microscopic analysis with a fibril-reinforced finite-element model, *J. Biomech.* 40 (2007) 1862–1870.
- [84] M.A. Biot, Theory of propagation of elastic waves in a fluid-saturated porous solid. II. Higher frequency range, *J. Acoust. Soc. Am.* 28 (1956) 179–191.
- [85] B.R. Simon, Multiphase poroelastic finite element models for soft tissue structures, *Appl.*

- Mech. Rev. 45 (1992) 191–218.
- [86] P. Julkunen, W. Wilson, H. Isaksson, J.S. Jurvelin, W. Herzog, R.K. Korhonen, A review of the combination of experimental measurements and fibril-reinforced modeling for investigation of articular cartilage and chondrocyte response to loading, *Comput. Math. Methods Med.* 2013 (2013).
- [87] M. Adouni, A. Shirazi-Adl, Evaluation of knee joint muscle forces and tissue stresses-strains during gait in severe OA versus normal subjects, *J. Orthop. Res.* 32 (2014) 69–78.
- [88] K.S. Halonen, M.E. Mononen, J.S. Jurvelin, J. Töyräs, R.K. Korhonen, Importance of depth-wise distribution of collagen and proteoglycans in articular cartilage—a 3D finite element study of stresses and strains in human knee joint, *J. Biomech.* 46 (2013) 1184–1192.
- [89] J.T.A. Mäkelä, S.K. Han, W. Herzog, R.K. Korhonen, Very early osteoarthritis changes sensitively fluid flow properties of articular cartilage, *J. Biomech.* 48 (2015) 3369–3376.
- [90] L.P. Li, J. Soulhat, M.D. Buschmann, A. Shirazi-Adl, Nonlinear analysis of cartilage in unconfined ramp compression using a fibril reinforced poroelastic model, *Clin. Biomech.* 14 (1999) 673–682.
- [91] W. Wilson, J.M. Huyghe, C.C. Van Donkelaar, A composition-based cartilage model for the assessment of compositional changes during cartilage damage and adaptation, *Osteoarthr. Cartil.* 14 (2006) 554–560.
- [92] J.T.A. Mäkelä, R.K. Korhonen, Highly nonlinear stress-relaxation response of articular cartilage in indentation: Importance of collagen nonlinearity, *J. Biomech.* 49 (2016) 1734–1741.
- [93] A. Benninghoff, Form and structure of hyaline cartilage in relation to function, *Erste Mitteilung Zeitschrift Für Anat. Und Entwicklungsgeschichte.* 76 (1925) 43–63.
- [94] A. Seifzadeh, J. Wang, D.C.D. Oguamanam, M. Papini, A nonlinear biphasic fiber-reinforced porohyperviscoelastic model of articular cartilage incorporating fiber reorientation and dispersion, *J. Biomech. Eng.* 133 (2011) 81004.
- [95] J.C. Lagarias, J.A. Reeds, M.H. Wright, P.E. Wright, Convergence properties of the Nelder--Mead simplex method in low dimensions, *SIAM J. Optim.* 9 (1998) 112–147.
- [96] J.T.A. Mäkelä, Z.S. Rezaeian, S. Mikkonen, R. Madden, S.-K. Han, J.S. Jurvelin, W. Herzog, R.K. Korhonen, Site-dependent changes in structure and function of lapine articular cartilage 4

- weeks after anterior cruciate ligament transection, *Osteoarthr. Cartil.* 22 (2014) 869–878.
- [97] R.Y. Hori, L.F. Mockros, Indentation tests of human articular cartilage, *J. Biomech.* 9 (1976) 259–268. doi:10.1016/0021-9290(76)90012-9.
- [98] J.S. Jurvelin, M.D. Buschmann, E.B. Hunziker, Optical and mechanical determination of Poisson's ratio of adult bovine humeral articular cartilage, *J. Biomech.* 30 (1997) 235–241.
- [99] R.C. Stewart, J.T.J. Honkanen, H.T. Kokkonen, V. Tiitu, S. Saarakkala, A. Joukainen, B.D. Snyder, J.S. Jurvelin, M.W. Grinstaff, J. Töyräs, Contrast-Enhanced Computed Tomography Enables Quantitative Evaluation of Tissue Properties at Intrajoint Regions in Cadaveric Knee Cartilage, *Cartilage.* 8 (2017) 391–399. doi:10.1177/1947603516665443.
- [100] R.E. Wilusz, S. Zauscher, F. Guilak, Micromechanical mapping of early osteoarthritic changes in the pericellular matrix of human articular cartilage, *Osteoarthr. Cartil.* 21 (2013) 1895–1903. doi:10.1016/j.joca.2013.08.026.
- [101] M. Wang, Z. Peng, J. Price, N. Ketheesan, Study of the nano-mechanical properties of human knee cartilage in different wear conditions, *Wear.* 301 (2013) 188–191. doi:10.1016/j.wear.2012.12.015.
- [102] F. Boschetti, G.M. Peretti, Tensile and compressive properties of healthy and osteoarthritic human articular cartilage, *Biorheology.* 45 (2008) 337–344. doi:10.3233/BIR-2008-0479.
- [103] F. Boschetti, G. Pennati, F. Gervaso, G.M. Peretti, G. Dubini, Biomechanical properties of human articular cartilage under compressive loads., *Biorheology.* 41 (2004) 159–166.
- [104] M.J. Nissi, J. Rieppo, J. Töyräs, M.S. Laasanen, I. Kiviranta, M.T. Nieminen, J.S. Jurvelin, Estimation of mechanical properties of articular cartilage with MRI - dGEMRIC, T2 and T1 imaging in different species with variable stages of maturation, *Osteoarthr. Cartil.* 15 (2007) 1141–1148. doi:10.1016/j.joca.2007.03.018.
- [105] L.A. Knight, S. Pal, J.C. Coleman, F. Bronson, H. Haider, D.L. Levine, M. Taylor, P.J. Rullkoetter, Comparison of long-term numerical and experimental total knee replacement wear during simulated gait loading, *J. Biomech.* 40 (2007) 1550–1558.
- [106] B.J. West, N. Scafetta, Nonlinear dynamical model of human gait, *Phys. Rev. E.* 67 (2003) 51917.
- [107] E.K. Danso, J.T.A. Mäkelä, P. Tanska, M.E. Mononen, J.T.J. Honkanen, J.S. Jurvelin, J. Töyräs, P. Julkunen, R.K. Korhonen, Characterization of site-specific biomechanical

- properties of human meniscus—Importance of collagen and fluid on mechanical nonlinearities, *J. Biomech.* 48 (2015) 1499–1507.
- [108] H. Pereira, S.G. Caridade, A.M. Frias, J. Silva-Correia, D.R. Pereira, I.F. Cengiz, J.F. Mano, J.M. Oliveira, J. Espregueira-Mendes, R.L. Reis, Biomechanical and cellular segmental characterization of human meniscus: building the basis for Tissue Engineering therapies, *Osteoarthr. Cartil.* 22 (2014) 1271–1281.
- [109] M.R. DiSilvestro, Q. Zhu, J.-K.F. Suh, Biphasic poroviscoelastic simulation of the unconfined compression of articular cartilage: II—Effect of variable strain rates, *J. Biomech. Eng.* 123 (2001) 198–200.
- [110] J. Makela, Structural and functional alterations of articular cartilage in osteoarthritis, 2016.
- [111] T. Niemelä, T. Virén, J. Liukkonen, D. Argüelles, N.C.R. te Moller, P.H. Puhakka, J.S. Jurvelin, R.-M. Tulamo, J. Töyräs, Application of optical coherence tomography enhances reproducibility of arthroscopic evaluation of equine joints, *Acta Vet. Scand.* 56 (2014) 3.